TECTONICS, VOL. 17, NO. 2, PAGES 203-220, APRIL 1998

Subsidence of a volcanic basin by flexure and lower crustal flow: The eastern Snake River Plain, Idaho

Nadine McQuarrie[1] and David W. Rodgers

Department of Geology, Idaho State University, Pocatello

Abstract. The Eastern Snake River Plain (ESRP) is a linear volcanic basin interpreted by many workers to reflect late Cenozoic migration of North America over the Yellowstone hotspot. Thermal subsidence of this volcanic province with respect to Yellowstone has been documented by several workers, but no one has characterized subsidence with respect to the adjacent Basin and Range Province. This paper documents crustal flexure along the northwest edge of the ESRP, uses flexure to model the dimensions of a dense load beneath the basin, and presents evidence in support of density-driven subsidence and lower crustal flow away from the basin. Crustal flexure adjacent to the ESRP is reflected by the attitudes of Mesozoic fold hinges and Neogene volcanic rocks. Fold hinges formed with a subhorizontal plunge and a trend perpendicular to the ESRP but now show a southward plunge near the ESRP of as much as 20°-25°. We present a contour map of equal fold plunges proximal to the ESRP that shows flexure is roughly parallel to and extends 10-20 km north of the average edge of the ESRP. Flexural profiles indicate the minimum amount of ESRP subsidence, with respect to the Basin and Range; subsidence ranges from 4.5 to 8.5 km. The structural contour map and published seismic and gravity data were used to develop and constrain flexural subsidence models. These models indicate the flexed crust is very weak (flexural parameter of 4-10 km), interpreted to be a result of the high heat flow of the ESRP. Assuming subsidence was induced by emplacement of a dense crustal layer beneath the ESRP, a midcrustal "sill" identified in previous seismic surveys is too wide and probably too thin to produce the measured flexure. New dimensions include a thickness of 17-25 km and a half width of 40-50 km, which place the edge of the sill beneath the edge of the ESRP. The dimensions of the ESRP sill are based on isostatic compensation in the lower crust because compensation in the asthenosphere requires an unreasonable sill thickness of 30+ km and because ESRP seismic, gravity, and heat flow data support lower crustal compensation. Density-driven lower crustal flow away from the ESRP is proposed to accommodate subsidence and maintain isostatic equilibrium. Timing of subsidence is constrained by ESRP exploratory wells, where 6.6 Ma rhyolites at a depth of 1.5 km indicate most subsidence occurred prior to their emplacement, and by strong spatial correlations between plunge contours and Quaternary volcanic rift zones. Two processes interpreted to contribute to the load include an extensive midcrustal mafic load emplaced at ~10 Ma, which provided the heat source for the initial rhyolitic volcanism on the ESRP, and continuing, localized loads from dikes and sills associated with Quaternary basalts. Widespread ~10 Ma magmatism and subsidence conflicts with simple time-transgressive migration of the Yellowstone hotspot, indicating a need for revision of the hotspot paradigm.

1. Introduction

Volcanic basins associated with migrating hotspots (and not associated rifting) are virtually unrecognized in the geologic literature [*Johnson*, 1989; *Allen and Allen*, 1990; *Busby and Ingersoll*, 1995], mainly because they hardly ever exist. One example may be the eastern Snake River Plain (ESRP), which is colinear with the Yellowstone Plateau and displays a northeastward progressing pattern of late Cenozoic silicic volcanism acompanied by a northeastward and outward progressing pattern of extension in the adjacent Basin and Range (Figure 1)[*Anders et al.*, 1989; *Pierce and Morgan*, 1992]. Time-transgressive tectonism has been attributed to the presence of the Yellowstone hotspot beneath a southwest migrating North American Plate [*Morgan*, 1972; *Armstrong et al.*, 1975; *Suppe et al.*, 1975; *Alt et al.*, 1988; 1990; *Rodgers et al.*, 1990; *Pierce and Morgan*, 1992], although other theories have been proposed [*Hamilton*, 1987, 1989; *Eaton et al.*, 1975; *Christiansen and McKee*, 1978]. Because controversy remains about the nature of plumes and hotspots, the term "hotspot" is used nongenetically in this paper and refers to the northeastward time-transgressive nature of both silicic volcanism and faulting. The ESRP itself is a long-lived basin as manifested by basin fill that includes several kilometers of rhyolite and basalt, its distinct topographic and structural depression, and subsidence that has lasted for millions of years.

Subsidence of the ESRP is due to several mechanisms. Thermal contraction in the wake of the Yellowstone hotspot is a widely accepted model supported by the present-day southwesterly decrease in ESRP elevation [*Brott et al.*, 1981; *Blackwell et al.*, 1992] and the analogous subsidence of oceanic hotspots [*Crough*, 1978; *Sleep*, 1987]. However, thermal contraction alone is an insufficient mechanism because of the measurable subsidence of the ESRP with respect to the surrounding Basin and Range Province despite average ESRP heat flow values that are 30% greater than those in the Basin and Range [*Blackwell et al.*, 1992]. Besides sediment and volcanic loading, another potential mechanism involves the emplacement of dense mafic magma [*Sparlin et al.*, 1982] into the ESRP middle crust, creating a load that subsides to

[1]Now at Department of Geosciences, University of Arizona, Tucson

paper number 97TC03762.
0278-7407/98/97TC-03762$12.00

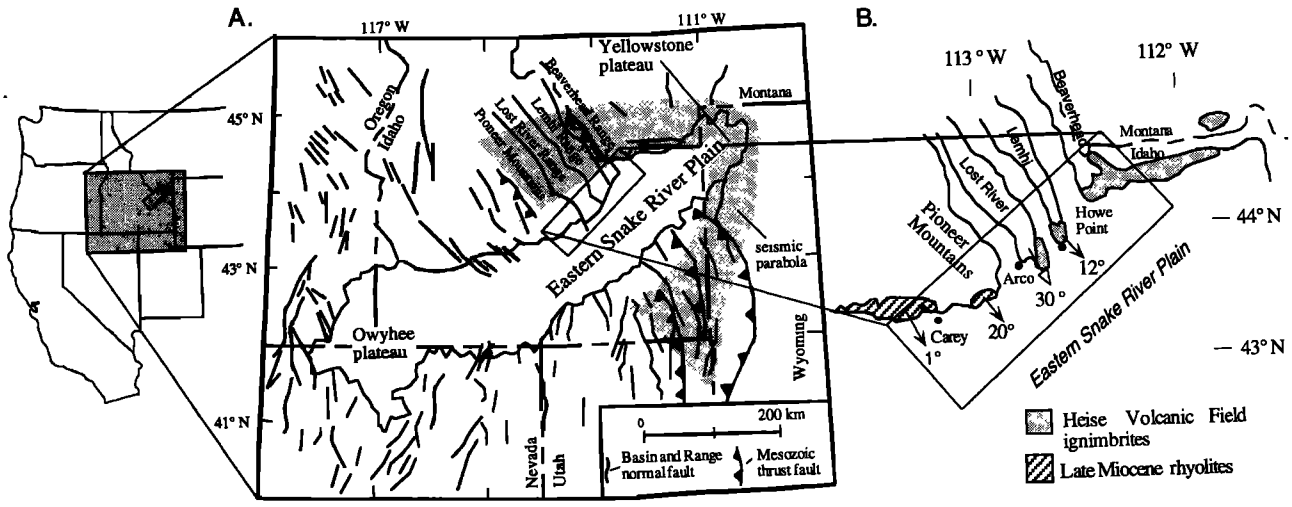

Figure 1. (a) Map of the western United States showing faults of the northeastern Basin and Range province, major Mesozoic thrust faults and the location of the eastern Snake River Plain, Yellowstone Plateau, and Owyhee Plateau. Figure 1 modified from *Rodgers et al.*[1990], with permission of the publisher, the Geological Society of America, Boulder, Colorado, USA, copyright © Geological Society of America.
(b) Map of northern ESRP region showing distribution of Neogene volcanic rocks and selected measurements of subsidence. Barbed arrows indicate dip of Neogene rocks; open arrows indicate plunge of Mesozoic fold hinges. Study area is outlined in box. Data are from *Schmidt* [1962], *Kuntz et al.* [1994b] and this study.

maintain isostatic equilibrium. To investigate mechanisms other than thermal contraction, this paper will focus on ESRP subsidence with respect to the adjacent Basin and Range. This "cross-axis" study, including the age, extent, and rate of subsidence of the ESRP volcanic basin, also has great potential for recording the space-time development of regional subsidence and magmatism.

Along the edges of the ESRP, the Basin and Range crust exhibits topographic flexure toward the ESRP [*Kirkham*, 1927, 1931; *Ruppel*, 1967; *Scott et al.*, 1985; *Rodgers et al.*, 1991; *Fritz and Sears*, 1993]. Interpreting this as crustal flexure due to subsidence of the ESRP, we have used Mesozoic fold hinges and Neogene volcanic rocks to quantify the three-dimensional flexural pattern along the northern edge of the ESRP. These data allow us to model crustal flexure adjacent to the ESRP and thus interpret the density, thickness, and strength of subsurface rocks. In particular, the extent of a dense mafic sill should be manifested by the extent of subsidence, while its density and thickness should be reflected by a specific amount of subsidence. Lithospheric strength should be reflected by the curvature of crustal flexure across the differentially subsided region. These results not only describe the style and geometry of basin subsidence but also have important implications for lower crustal flow and time-transgressive passage of the Yellowstone hotspot.

2. Geology of the Study Area

The study area is a rectangular zone about 40 by 150 km along the northern border of the ESRP that encompasses the Pioneer Mountains, Appendicitis Hills, Lost River Range, Lemhi Range, and Beaverhead Range (Figure 1). Here the upper crust is composed of Archean or Middle Proterozoic crystalline basement, an 8-13+ km thick sequence of Late Proterozoic to Permian marine sedimentary rocks, localized Paleogene plutonic and volcanic rocks, and Neogene volcanic and sedimentary rocks.

During late Mesozoic time, flat-lying sedimentary rocks were extensively shortened along east vergent folds and thrusts [*Armstrong and Oriel*, 1965; *Royse et al.*, 1975)]. Fold location, style and geometry were documented by previous mapping in the area [*Beutner*, 1968; *Garmezy*, 1981; *Scott*, 1982; *Skipp*, 1988, 1989; *Skipp et al.*, 1990; *Skipp and Bollmann*, 1992; *Kuntz et al.*, 1994a]. Generally, folds are located in the incompetent limestone units of the Mississippian through Permian formations, and most folds are map scale with wavelengths ranging from 250 to 3000 m. Fold hinges trend perpendicular to the ESRP (Figure 2).

Paleogene volcanism was accompanied by NW-SE crustal extension [*McIntyre et al.*, 1982; *Janecke*, 1992]. Tilting of the fault blocks associated with rotational faulting was documented north of but not within the study area [*Janecke*, 1992].

Neogene volcanic rocks are present at Howe Point in the south tip of the Lemhi Range. The rocks include two members of the Heise Volcanic Group, the 6.0 Ma tuff of Blue Creek and the 6.6 Ma tuff of Blacktail, both densely welded, rhyolite ash flow tuffs derived from vents on the ESRP [*Morgan et al.*, 1984]. Their proximal facies have been interpreted to indicate eruption from nearby vents [*Morgan et al.*, 1994], and they are part of the time-transgressive sequence of silicic volcanic rocks that mark the inferred passage of the Yellowstone hotspot. Neogene rhyolite was encountered by drilling on the ESRP between depths of 1 and 3.1 km [*Doherty et al.*, 1979)], and relatively low-density rock (rhyolite?) was interpreted using wide-angle seismic refraction to extend to 8 km depth beneath the ESRP [*Sparlin et al.*, 1982].

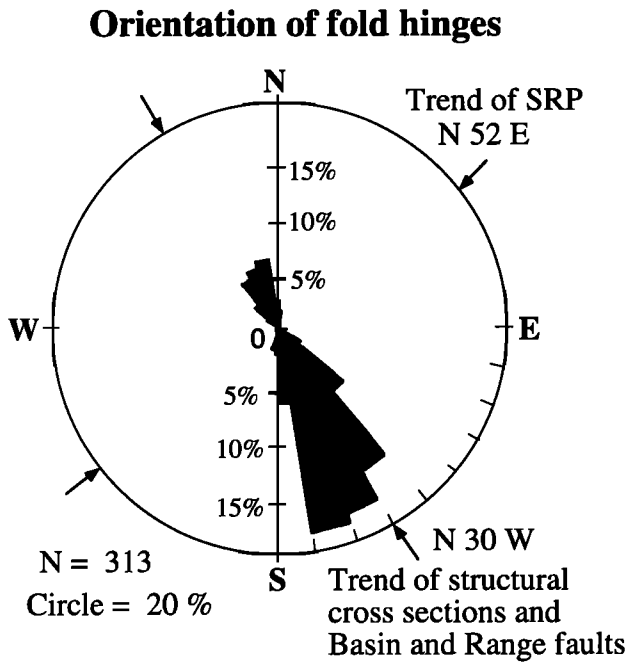

Figure 2. Rose diagram of plunge direction of 313 fold hinges showing consistent north-northwest / south-southeast trend and high percentage of southeast plunging folds.

Pliocene-Quaternary basalt covers the surface of the ESRP everywhere [*Kuntz et al.*, 1992]. Basalt is typically olivine tholeiite that forms individual flows several meters thick and a cumulative thickness on the ESRP of about 1000 m. Surface basalts are younger than 1 Ma, whereas subsurface basalts may be as old as 4 Ma.

Neogene-Quaternary deformation consists of crustal flexure or downwarping (discussed in section 3) and crustal extension. No record of Neogene extension is preserved on the ESRP, but Quaternary extension is shown by several volcanic rift zones that trend NNW, perpendicular to the regional extension direction. The amount of Quaternary extension is undocumented but inferred to be approximately similar to the adjacent Basin and Range [*Rodgers et al.*, 1990]. North of the ESRP, three main range-bounding, half graben faults accommodate northeast to southwest Basin and Range extension. All three faults dip moderately southwest, are approximately 120 km in length and include several short segments that are distinguished by different geomorphic expressions, structural relief, and ages of last movement [*Scott et al.*, 1985; *Turko and Knuepfer*, 1991]. Structural relief and recent fault activity along the three faults is greater on the central segments and gradually decreases toward the tips [*Pierce and Morgan*, 1992]. Studies by *Bruhn et al.* [1992] and D. Wu and R.L. Bruhn [Structural and rupture characteristics of the southern Lost River fault zone, Idaho, informal report prepared for Woodward-Clyde Federal Services, Oakland, Ca., 33 pp., 1994.] suggest the southern tips extend into the ESRP and are now zones of inactive or diminished faulting (Lemhi fault) or represent a transition zone between faulting and volcanic rift zones (Lost River fault). Basin and Range faulting began in the mid-Miocene, as evidenced by tilted basin fill in Birch Creek Valley [*Rodgers and Anders*, 1990], and continues today as demonstrated by fault scarps and the 1983 Borah Peak earthquake [*Scott et al.*, 1985; *Smith et al.*, 1985].

The pattern of active faulting is part of a more widespread zone referred to as the seismic parabola [*Anders et al.*, 1989] (Figure 1). This zone of significant seismicity, Quaternary faulting, and elevated topography [*Scott et al.*, 1985; *Anders et al.*, 1989; *Pierce and Morgan*, 1992] strongly contrasts with the ESRP and flanking Basin and Range where seismicity is negligible and elevations are relatively low. To produce the observed mechanical behavior of the aseismic "interior zone," workers have proposed that it was strengthened by various processes including lithospheric cooling [*Anders and Sleep*, 1992], the emplacement of a midcrustal mafic sill [*Sparlin et al.*, 1982; *Anders and Sleep*, 1992], the emplacement of subcrustal to lower crustal mafic rock [*Pierce and Morgan*, 1992], or dehydration of lower crust [*Pierce and Morgan*, 1992]. *Parsons and Thompson* [1991] have attributed the interior zone to suppressed differential stresses due to mafic dike injection.

3. ESRP and Basin and Range downwarping

Subsidence along the axis of the ESRP as a function of increasing distance from the Yellowstone plateau was documented by *Reilinger et al.* [1977] and modeled as thermal contraction [*Brott et al.*, 1981; *Blackwell et al.*, 1992] or as a relative increase in loading by dense magmatic intrusions [*Anders and Sleep*, 1992]. Cross-axis subsidence and the subsequent flexure or downwarping of the adjacent Basin and Range was first described by *Kirkham* [1927, 1931], who recognized that Neogene rocks within 10-20 miles of the ESRP dip 4°-5° toward it, with local dips as great as 5°-20°. Kirkham also described ridge elevations of the adjacent Basin and Range that decrease toward the ESRP. Additional evidence of downwarping cited by Kirkham and other authors includes (1) an axial drainage system in the Basin and Range where rivers flow toward the ESRP, (2) drainage reversals within the basins flanking the ESRP [*Ruppel*, 1967; *Rodgers et al.*, 1991; *Fritz and Sears*, 1993], (3) ridgecrest elevations that decrease toward the ESRP, (4) basin floor elevations that slope toward the ESRP, (5) Neogene rocks which have a component of dip toward the ESRP [*Rodgers and Anders*, 1990], (6) Mesozoic fold hinges that plunge gently toward the ESRP, and 7) a diffuse zone of northeast striking normal faults accommodating minor SE-NW extension due to crustal flexure [*Zentner*, 1989a; *Rodgers and Zentner*, 1988]. Although these workers used topographic and geologic features to identify localized subsidence of the ESRP or downwarping of the Basin and Range, the amount and distribution of structural downwarping throughout the region remains unmeasured.

4. Structural Analysis of Downwarping

4.1 Topographic Downwarp

Ridge crest profiles of the mountain ranges north of the ESRP reflect both uplift along the range-bounding faults and flexural response to ESRP subsidence. The profiles of the three main mountain ranges north of the ESRP were plotted to

estimate the amount and extent of downwarping simply by measuring elevation changes. The topographic profiles of the ridges were constructed by plotting the elevations of the ridge crests in map view at a scale of 1:24,000. The cross sections were then condensed and plotted with a vertical exaggeration of three times (Figure 3).

These data show that the topographic downwarp extends from the ESRP to 20 km north of the range tips, with the ridge crests plunging 5° toward the ESRP. Elevation difference between the ranges and the ESRP is approximately 1.5 km.

4.2 Structural downwarp

4.2.1. Data. Orientations of Paleozoic sedimentary beds that define a Mesozoic fold were measured in the field and plotted on a lower hemisphere, equal-area projection to determine the trend and plunge of each fold. Compilation of 313 folds indicates a regular pattern of orientations: fold hinges trend southeast, approximately perpendicular to the trend of the ESRP (Figure 2), plunge 0°-25° southeast, and show progressively increasing plunge to the southeast.

The orientations of compaction foliations in the tuff of Blue Creek and the tuff of Blacktail were measured at Howe Point (Figure 1), with the emphasis on the change in strike over a north to south transect. There is a noticeable change from a northwest strike in the north to a more northerly strike in the south. This progressive change in strike and southward steepening dip indicates the presence of a very gentle fold with a northeast trending hinge and a southerly limb that dips 12°.

4.2.2. Data reduction. Tilted attitudes of fold hinges and compaction foliation may reflect the separate or cumulative effects of several processes including (1) initial nonhorizontal deposition or formation, (2) northeastward tilting due to Basin and Range half graben faults, (3) tilting due to differential slip along major Basin and Range faults, and (4) downwarp-induced tilting. Tilting due to the first three processes must be identified and removed to correctly assess the latter process. As discussed below, we conclude that tilting indicated by fold hinges and compaction foliation provides an accurate record of downwarping.

Paleozoic rocks were undeformed prior to Cretaceous shortening, so that fold hinges should have formed with subhorizontal plunges [*Woodward et al.*, 1985]. Independent support for this is given by paleogeologic maps of the study area, which reconstruct the pre-Tertiary geology based on the map-scale distribution of rocks below the Tertiary unconformity. On the basis of widespread distribution of Mississippian (to the west) and Permian (to the east) strata, the study area was interpreted to display negligible structural relief in a north-south direction, with no evidence of fault-bend folds over lateral thrust ramps [*Rodgers and Janecke*, 1992].

Compaction foliation in the basal vitropheres of the ash flow tuffs is inferred to reflect original horizontality based on consistent measurements over a 9 km^2 region and on a comparative study of tilts recorded by direct measurement and paleomagnetic inclination [*Anders et al.*, 1989; *Rodgers and Anders*, 1990].

Basin and Range fault-induced tilting of footwall rocks is certain throughout the area. Halfgraben faults uniformly dip west to southwest, and tilt rocks and structures dip 5°-20° to the east-northeast [*Scott et al.*, 1985; *Smith et al.*, 1985].

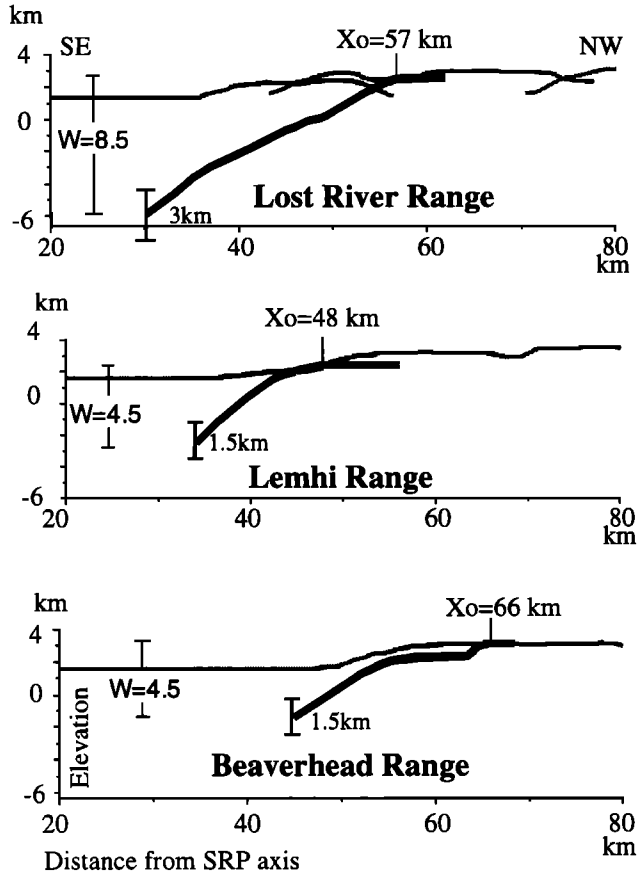

Figure 3. Cross sections of structural downwarping and topography. Elevations of the ranges were projected on a straight vertical plane and averaged over 6 km to smooth out small irregularities. There is a vertical exaggeration three times. The structural cross section show more extensive downwarping and greater subsidence than that indicated by topography. The vertical distance between the zone of 0° plunges and the depth of the final plunge at the edge of the plain is the minimum amount of subsidence equal to *W*. *Xo* is edge of basin measured from the eastern Snake River Plain axis. Line of section is located on Figure 4.

Fortunately, the tilt direction is perpendicular to the trend of the fold hinges, leaving their orientations virtually unaffected. However, tilting due to Basin and Range faulting was removed from the Neogene volcanic rocks to isolate the amount of downwarping.

Tilting due to differential slip along the strike of individual Basin and Range faults is less obvious. The major Basin and Range faults north of the ESRP have larger offsets in the centers than along the tips [*Scott et al.*, 1985]. The larger offsets bow the ranges producing slight down-to-the-north tilting of the hanging wall rocks and down-to-the-south tilting of footwall rocks in the study area. If the entire height of the ranges were produced by differential uplift along the 30 km length of the study area, this uplift has a potential to increase (or decrease) the plunge values by a maximum of 3°. However, fault offset is not essentially zero at the ESRP border [*Bruhn et al.*, 1992], decreasing the amount of fault-generated plunge to < 3°, which is below the resolution of the data as discussed

below. A stronger argument for disregarding differential uplift takes into account the half graben style of faulting in the area. In halfgraben faulting, north-south tilting due to differential slip should be essentially zero at the east-west midpoint in each fault block, which roughly corresponds to the intersection of the valley floor with bedrock on the eastern side of each range. In the study area, plunge values on the eastern and western sides of the ranges are comparable, with no reduction in plunge values at the midpoint, evidence that tilting due to differential uplift is negligible.

4.2.3. Statistical analysis. Fold data are not uniformly distributed throughout the study area, so the data were contoured to understand the regional pattern of fold plunges. Folds in each map section grid (1.7 km^2) were counted and averaged with the folds contained in a 15.3 km^2 grid around it, similar to the technique used to contour data on a lower hemisphere equal-area projection. This running statistical average was taken for each section grid to smooth out irregularities, to emphasize overall trends, and to provide numerical values for areas with no measured folds. The standard deviation of the average plunge was calculated to be ±3°. The resulting map of average fold plunges was then contoured in 5° increments, using the interpretive contouring method. Contour lines measured between data points are expressed as solid lines. Contours that are extrapolated between areas of data points are dashed (Figure 4).

To show two-dimensional profiles of downwarping recorded by the fold hinges, structural cross sections were drawn perpendicular to the trend of the ESRP along the ridge crests of the Lost River, Lemhi, and Beaverhead Ranges (Figure 3). For each cross section, the plunge represented by each contour was projected to the location of the next contour, producing small zones of discrete plunges (Figure 5). The final plunge (measured at the tips of each range) was projected a minimal amount of 3 km under the ESRP. The plunges were connected and smoothed to form a hypothetical curved line that represents downwarped Basin and Range crust. Figure 5 shows the two end-member curves represented by the ± 3° standard

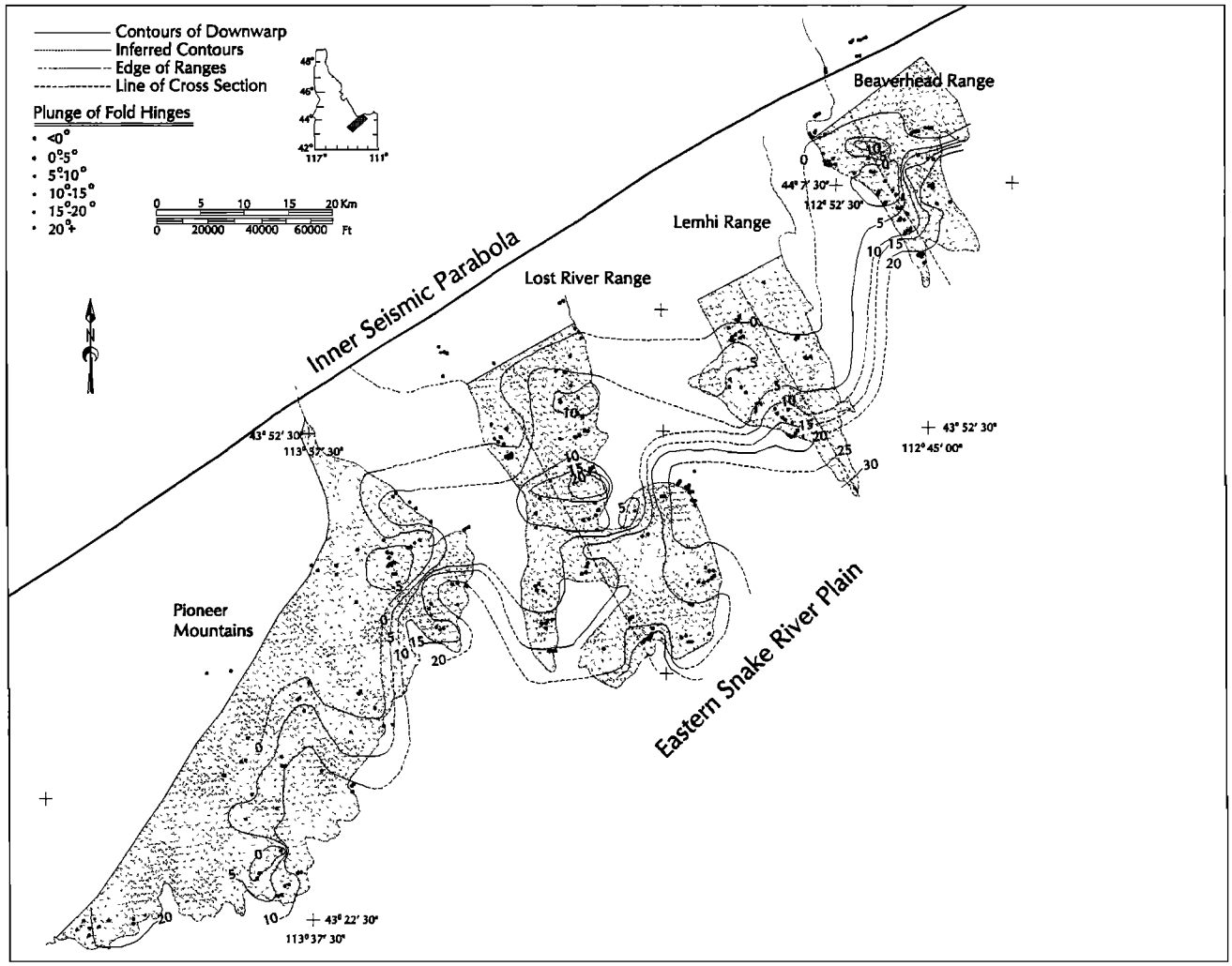

Figure 4. Contour map of equal plunges within the Basin and Range crust adjacent to the eastern Snake River Plain indicating amount and extent of downwarp. Contours represent degree of fold hinge plunge. Solid lines indicate contour lines measured between data points; dashed lines indicate contours that are extrapolated between areas of data points.

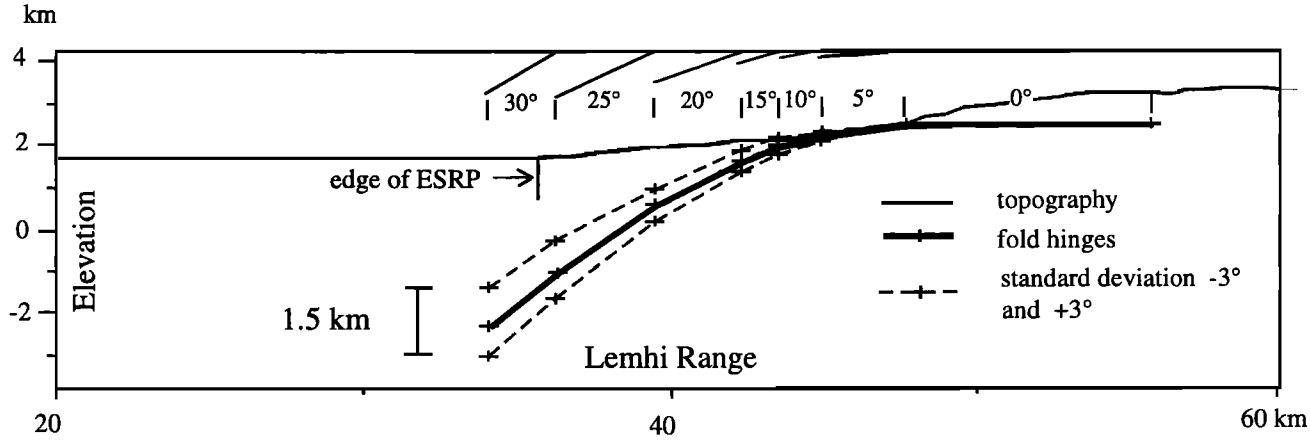

Figure 5. Cross section of structural downwarping and topography for the Lemhi Range. There is a vertical exaggeration of three times. Dashed lines indicate the margin of error associated with a standard deviation of ±3°. Locations of contour lines, indicated by short vertical lines, bracket zones of equal plunge. Thin angled lines represent actual plunge values for each contour. The final plunge value (30°) was projected 3 km under the ESRP. The error associated with the minimum amount of subsidence is 1.5 km.

deviation for the Lemhi Range. This deviation produces a 1.5 km error bar for the Lemhi and Beaverhead Ranges and a 3 km error bar for the Lost River Range.

4.2.4. Results. The map of contoured fold hinges shows a consistent pattern throughout the study area (Figure 4). The contour lines roughly parallel the axis of the ESRP and define a narrow downwarped zone, 20-35 km wide, that extends approximately 10-20 km north of the average edge of the ESRP. They also show a definite southeast increase in the southeastern plunges to a maximum of 25°. There is a general consistency in the spacing of the contours at the tip of the Lemhi and Beaverhead Ranges. The Lost River Range is unique, with the Arco Hills fault block displaying a wide, uniform dip of 20° to 25°. Each of the ranges shows discrete zones of increased plunge, usually between the 0° and 10° contour, represented by closed contours. These anomalous zones are roughly colinear, suggesting a geologic or tectonic significance; however, they do not appear to have any correlation with any previously mapped rock type, segment boundary, or cross fault.

The zone of structural downwarp is consistently located with respect to other structural domains. Most of the downwarped zone occurs within the southernmost (inactive) segment boundaries of the range-bounding faults. The 0° contour is roughly coincident (within 10 km) with the inner parabola of *Anders et al.* [1989] (Figure 4). The zone of downwarping indicated by the contour map also contains the zone of ESRP parallel normal faults distinguished by *Zentner* [1989b], who believed they formed because of flexure of the Basin and Range crust.

A second-order trend is the prominent pattern of recessions and salients that give a scalloped appearance to the contours. The recessionals make sharp curves inward on both the ranges (Pioneer Mountains and the Appendicitis Hills) and the intervening valleys (Little Lost River Valley and Birch Creek Valley) and exhibit both closely and widely spaced contours (Figure 4).

Structural cross sections (Figures 3 and 5) show that measured structural relief due to downwarping is much greater than the 1.5 km indicated by topographic relief and that the structural surface delineated by plunge values does not parallel topography. Structural relief ranges from 4.5 to 8.5 km, depending upon the cross section, an amount which represents the minimum ESRP subsidence with respect to the Basin and Range. In addition, the zone of structural downwarping extends as much as 10 km north of the topographical downwarp, indicating that the topographic downwarp represents only a portion of the actual crustal downwarp.

4.2.5. Interpretation. The pattern of subsidence and downwarping indicates that a laterally extensive, crustal- to lithospheric-scale process has affected the region. Regional subsidence is attributed to the emplacement of a load on or beneath the ESRP and subsequent isostatic compensation resulting in relative subsidence of the ESRP. A load consists of one or more crustal layers that are thicker or more dense than adjacent crustal layers. One way to increase density is to reduce volume through thermal contraction. For the subsidence of the ESRP to be caused by thermal contraction alone, the adjacent Basin and Range would need to have a higher heat flow than the ESRP. However, *Blackwell et al.* [1992] reported that the heat flow in the northern Basin and Range is variable but averages about 80 mWm^{-2}, much lower than the 107 mWm^{-2} heat flow of the ESRP [*Blackwell et al.*, 1992]. Thermal contraction, although a viable process along the length of the ESRP, is insufficient to cause subsidence with respect to the Basin and Range.

The 5-8 km thick upper layer of relatively low density (2.5 g cm^{-3}) basalts, sediments and rhyolites on the ESRP [*Sparlin et al.*, 1982] was hypothesized to be the "load" that induced ESRP subsidence [*Kirkham*, 1927, 1931]. According to subsidence models [*Turcotte and Schubert*, 1982], surficial loading alone will yield both subsidence of the basin floor and an increase in topographic elevation, because of thickening of the buoyant upper crust. This indicates that if the structural

subsidence of the ESRP was only due to loading by basalts, sediments, and rhyolites, then the ESRP should be a topographic high rather than a depression. However, the redistribution of material from within the ESRP to the surface would have a noticeable effect on an upper crustal structural horizon.

Another "load" previously proposed to produce ESRP subsidence is dense mafic rock within the crust created by ponding of magmas [*Anders and Sleep*, 1992]. Authors have proposed that dense layers exist within the ESRP crust, either in the lower crust [*Leeman*, 1982a] or middle crust [*Sparlin et al.*, 1982; *Greensfelder*, 1981; *Anders and Sleep*, 1992]. A middle to lower crustal load of dense material could produce both structural and topographic subsidence of the ESRP and is favored in this paper.

5. Flexural Modeling

5.1. Selection of the Model

The purpose of modeling flexure is to test the hypothesis that previously described dense crustal layer(s) beneath the ESRP (Figure 6) could generate the appropriate load to produce the downwarping measured in this study. If this hypothesis is proven invalid, flexural modeling can provide a range of new load dimensions that could produce the measured downwarp, as well as estimates of crustal strength and depth of compensation.

Geological and geophysical investigations of the ESRP indicate it is underlain by several continuous subhorizontal lithologic layers, including (from top to bottom) (1) Pliocene to Holocene basalt flows with a veneer of loess, sand dunes and alluvial and lacustrine sediments [*Malde*, 1991; *Kuntz et al.*, 1992] and intercalated sediments that form a layer about 1 km thick [*Doherty et al.*, 197]; (2) Neogene rhyolite encountered by drilling to a depth of 3.1 km [*Doherty et al.*, 1979] and interpreted by wide-angle seismic refraction to extend to 8 km [*Sparlin et al.*, 1982]; (3) a mafic (gabbro?) layer from 8-20 km, commonly referred to as a midcrustal sill [*Sparlin et al.*, 1982]; (4) a lower sialic crust at 20-40 km; and (5) mantle below approximately 40 km [*Greensfelder*, 1981; *Sparlin et al.*, 1982; *Braile et al.*, 1982]. The Moho is interpreted to have no more than 1 km of relief beneath the ESRP and proximal Basin and Range [*Sparlin et al.*, 1982; *Peng*, 1996].

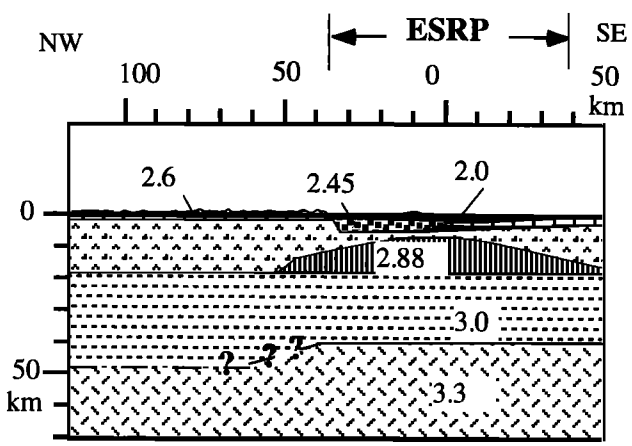

Figure 6. Crustal and upper mantle model of the ESRP and adjacent Basin and Range from seismic and gravity surveys after *Sparlin et al.* [1982]. There is no vertical exaggeration. Densities are in g cm^{-3}.

Table 1. Variables Used in Subsidence Modeling

Symbol	Name	Value	Reference
W	amount of subsidence or basin depth (km)	to be determined	
α	flexural parameter	to be determined	
hL	height of load (km)	to be determined or 12 km	1
L	half width of load	to be determined or 52 km	1
Xo	half width of basin (km)	47-66 km	2
ρ_s	density of basin fill		1
	basalt+sediments (1km)	2.0 g cm^{-3}	
	rhyolite (2km)	2.45 g cm^{-3}	
	rhyolite (2km)	2.55 g cm^{-3}	
	basin (5km)	2.40 g cm^{-3}	
ρ_c	density of upper crust	2.67 g cm^{-3}	1
ρ_{lc}	density of lower crust	3.0 g cm^{-3}	1
ρ_a	density of asthenosphere	3.3 g cm^{-3}	1
ρ_L	density of load	2.88 g cm^{-3}	1

Data references are as follows: 1, *Sparlin et al.* [1992]; 2, this study.

The crustal structure of the ESRP is similar to an elongate subsiding trough such as an aulacogen. Flexure adjacent to an aulacogen was modeled by *Nunn and Aires* [1988], who studied the Amazon Basin and identified a high-density intrusion at depth. Similar to the aulacogen model, the ESRP is interpreted to be underlain by a high-density intrusion, the midcrustal sill. The major difference between these two models is that the aulocagen is thinned by extension relative to adjacent crust, whereas the ESRP is unextended relative to the Basin and Range. We present a modified version of the aulocagen model to determine if the minimum amount of subsidence measured for the ESRP is compatible with the dimensions of the midcrustal mafic intrusion modeled by *Sparlin et al.* [1982]. The flexural model variables (Table 1) and equations are presented by *Angevine et al.* [1990]. The rectangular load flexure equations are as follows:

$$W(x=0) = (hL(\rho_L-\rho_c)(1-\exp(-L/\alpha)\cos(L/\alpha))/(\rho_{lc}-\rho_s)$$

$$W(0<x<L) = [(\rho_L hL)/2(\rho_{lc}-\rho_s)][2-(\exp-((L+x)/\alpha)(\cos((x+L)/\alpha)]$$

$$-[(\exp((-L-x)/\alpha)(\cos((L-x)/\alpha)]$$

$$W(x>L) = [(\rho_L hL)/2(\rho_{lc}-\rho_s)]\ [(\exp((-L-x)/\alpha)(\cos((L-x)/\alpha)]$$

$$-\ [(\exp((-L+x)/\alpha)(\cos((L+x)/\alpha)]$$

$$\alpha = (Xo-L)/[\cos^{-1}(\exp(-2L/\alpha)(\cos(Xo+L/\alpha)]$$

$$D = (\alpha^4(\rho_{lc}-\rho_s)g/4)$$

The seismic refraction and gravity data provide thicknesses and densities of the crustal layers. Subsidence equations are then used to calculate the flexural parameter α, flexural rigidity D, the amount of deflection (subsidence) of the ESRP, and the predicted shape of the flexed Basin and Range crust. The subsidence equations account for and remove the effect of subsidence due to volcanic basin fill to isolate the influence and, subsequently, the proportions of the proposed midcrustal sill.

Flexure modeling works under the following assumptions: (1) A portion of the lithosphere can be modeled as an elastic solid. (2) Vertical deflections are assumed to be small compared with the horizontal dimensions of the plate. (3) The elastic lithosphere is assumed to be thin compared to the horizontal dimensions of the plate. (4) Planar sections within the plate are assumed to remain planar after deflection. (5) The load is modeled as a midcrustal rectangular load. This assumption varies from the lenticular midcrustal sill proposed by *Sparlin et al.* [1982] (Figure 6), but matches the rectangular load imaged by *Peng* [1996].

Subsidence is modeled with compensation in both the asthenosphere and the lower crust, with the assumption that lower crustal flow has gone to completion [*Kaufman and Royden*, 1994]. Compensation in the lower crust or the asthenosphere is in reference to what is being displaced, lower crust with a density of 3.0 g cm^{-3} or asthenosphere with a density of 3.3 g cm^{-3}. Compensation in the lower crust is supported by a flat Moho [*Sparlin et al.*, 1982; *Peng*, 1996], a close relationship between topography and Bouguer gravity suggesting compensation by plastic flow within the upper 20 km of the crust [*Eaton et al.*, 1978], a high heat flow sufficient for partial melting or subsolidus grain-boundary relaxation of the lower crust [*Greensfelder*, 1981, *Blackwell et al.*, 1992], and geologically reasonable conclusions [*Sparlin et al.*, 1982; *Greensfelder*, 1981; *Blackwell et al.*, 1992].

The reference elevation of the flexure curves, relative to geography, is the eastern edge of each mountain range coincident with the elevation of the valley floors, because this is the median elevation of the east tilted Basin and Range fault blocks. The northern edge of the ESRP basin is defined as the edge of the flexed Basin and Range crust, coincident with the 0° contour (Figure 4).

5.2. Results of Modeling

We first use flexure modeling to test if the midcrustal sill defined by *Sparlin et al.* [1982] could produce the measured flexure and subsidence (Figure 7). The variables that are known are the thickness, extent, and density of the midcrustal sill, while the unknown variables are the half width of the basin (distance from the axis of the ESRP to the 0° contour), the shape of the flexed crust, and the amount of subsidence. The theoretical curves produced by the flexure equations are compared to the actual flexure curves described by the fold hinges to see if they match both the edge and shape of the flexed crust (Figure 3). Compensation of the load in the asthenosphere produces broad, shallow curves that have little resemblance to the measured flexure (Figure 7b). Compensation of the load in the lower crust, with a very weak crust (flexural parameter = 5 km), produces a similar curve but a

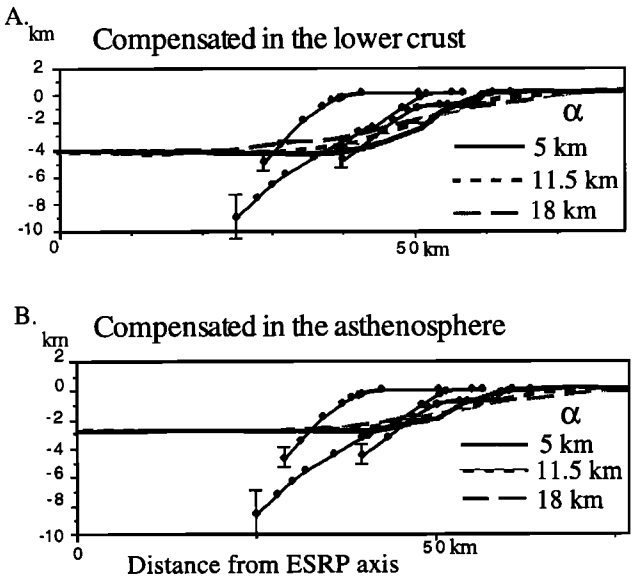

Figure 7. Actual flexure curves of the Lost River, Lemhi, and Beaverhead Ranges (Figure 3) compared to modeled curves using the parameters proposed by *Sparlin et al.* [1982]. These parameters include a load thickness of 12 km and a load half width of 52 km. The modeled curves represent different values of α, varied between 5 and 18 km. (a) Compensation in the lower crust yields a basin depth of 4.2 km, and (b) compensation in the asthenosphere yields a basin depth of 2.8 km. Both curves show a modeled basin much wider than the measured basin. Error bars show a 1.5-3 km range for minimum subsidence.

shallower basin (Figure 7a). The modeled depth of the basin is within 1 standard devition of the measured basin depth; however, the measured flexure defines a basin whose edge is significantly more proximal to the ESRP and whose base is deeper than that modeled using the layering scheme of *Sparlin et al.* [1982](Figure 7).

Although the density layering proposed by *Sparlin et al.* [1982] yields a basin depth within the upper limits of measured depth, the width of the load they propose is too great to produce the measured flexure. Instead, the measured flexure (Figure 3) and flexure equations can be used to model the load dimensions needed to match the shape of the flexed crust. In this inverse problem, the half width of the basin, the shape of the flexed crust, and the minimum amount of subsidence are known from the extent, amount, and shape of the downwarp described by the isoplunge contour map (Figure 4). The unknown variables determined by modeling are the width, density and thickness of the load, and the total amount of subsidence. In this model, compensation in the lower crust versus asthenosphere does not affect the shape of the curve. However, by compensating the load in the asthenosphere, the thickness of the load needed to produce the minimum amount of subsidence increases to geologically unreasonable values of 30+ km. Theoretical flexure curves assuming compensation in the lower crust are shown in Figures 8-10 and compared with the actual crustal flexure. Solutions for two independent variables (α and Wo) can be determined from the model.

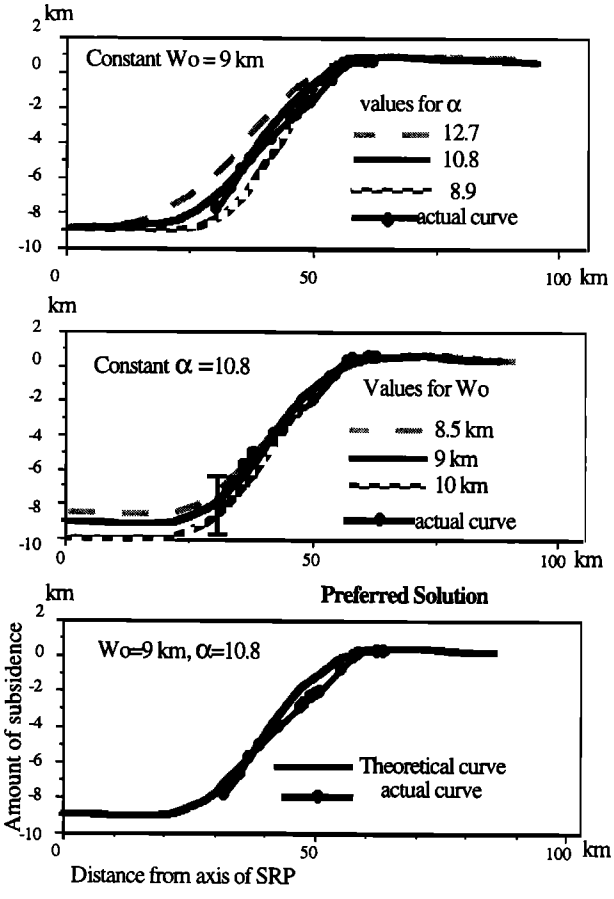

Figure 8. Actual and calculated flexural subsidence curves for the southern Lost River Range. Location of profile is shown in Figure 4. The half width of the midcrustal sill was varied between 30 and 50 km corresponding to a variation in α of 12.7-8.9 km. The depth of the basin was varied between 8.5 km and 10 km. Error bar shows a 3 km range in depths. The preferred solution is *Wo*= 9 km, *hL*= 25 km, α= 10.8 km, and *L*= 40 km.

Estimates for the flexural parameter α are strongly dependent on values chosen for the half width of the load. Likewise, the basin depth *Wo* is strongly dependent on the density and thickness of the load. To produce a close match between theoretical and actual flexure curves, a midcrustal sill must have a half width of 40-50 km, roughly coincident with the borders of the ESRP, and a thickness which ranges from 17 to 25 km with an average density of 2.88 g cm^{-3} (Figure 11). The minimum thickness of the load, to match the upper limit allowed by the standard deviation in plunge measurement, ranges from 10 to 19 km. However, as shown on Figures 8-10, the modeled flexure for minimum loads (low values of *Wo*) deviates from the measured flexure in the lower portions of the curves. If the crust were to decrease in strength again at the ESRP border, the thickness of the load would still need to be great enough to produce the measured flexure. However, the tail end of the curves produced purely by the model may be a lot steeper, lessening the thickness needed to pull down the plate from 4.5 to 6 km. Figure 12 shows other possible density-thickness combinations for the ESRP.

We note that the calculated strength of the crust (α = 5-10 km) is very low, which agrees with the high heat flow of the area and the sharp compositional boundary. Flexural parameters (α) of 5-10 km are slightly lower than the ~12 km calculated by *Anders et al.* [1993], who studied flexure of Basin and Range fault blocks immediately north of the study area. However, values of α that range from 5 to 10 km and the associated effective elastic thicknesses (EET) of 0.5 to 2 km are significantly lower than the EET of 6 km determined by coherence of gravity and topography over the ESRP/ Basin and Range transition [*Lowry and Smith*, 1995]. The above values all suggest the crust weakens toward the ESRP and may even drop in strength again under the ESRP to agree with differences in earthquake depths between the Basin and Range and ESRP [*Jackson et al.*, 1993; *Smith et al.*, 1989].

6. Gravity Modeling

Gravity modeling was completed to verify that the modified density layering determined by flexure modeling is consistent

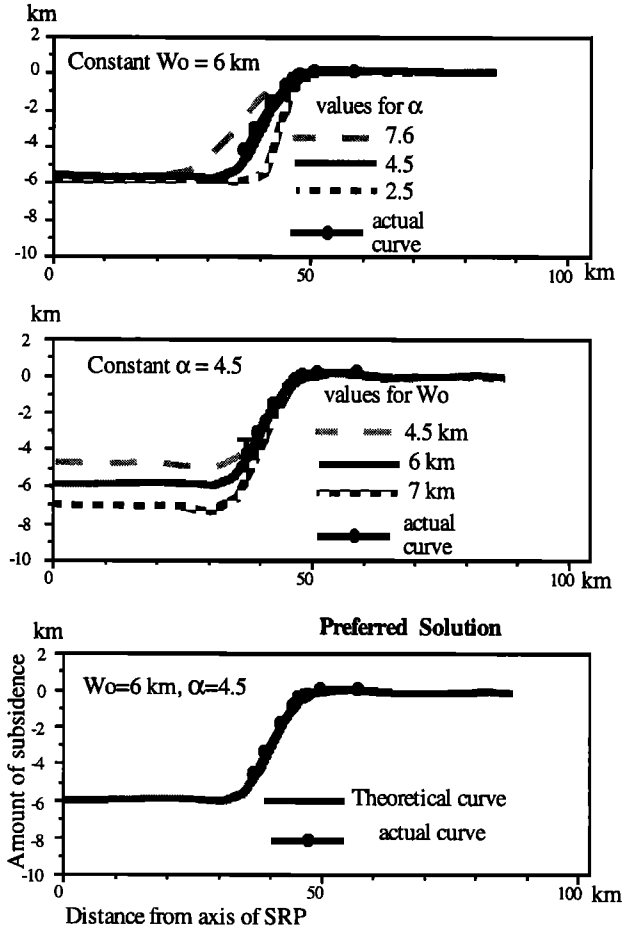

Figure 9. Actual and calculated flexure subsidence for the southern Lemhi Range. Location of profile is shown in Figure 4. The half width of the midcrustal sill was varied between 30 and 43 km corresponding to a variation in α of 7.6- 2.5 km. The depth of the basin varied between 4.8 and 7 km. Error bar shows a 1.5 km range in depths. The preferred solution is *Wo*= 6 km, *hL*= 17 km, α= 4.5 km, and *L*= 40 km.

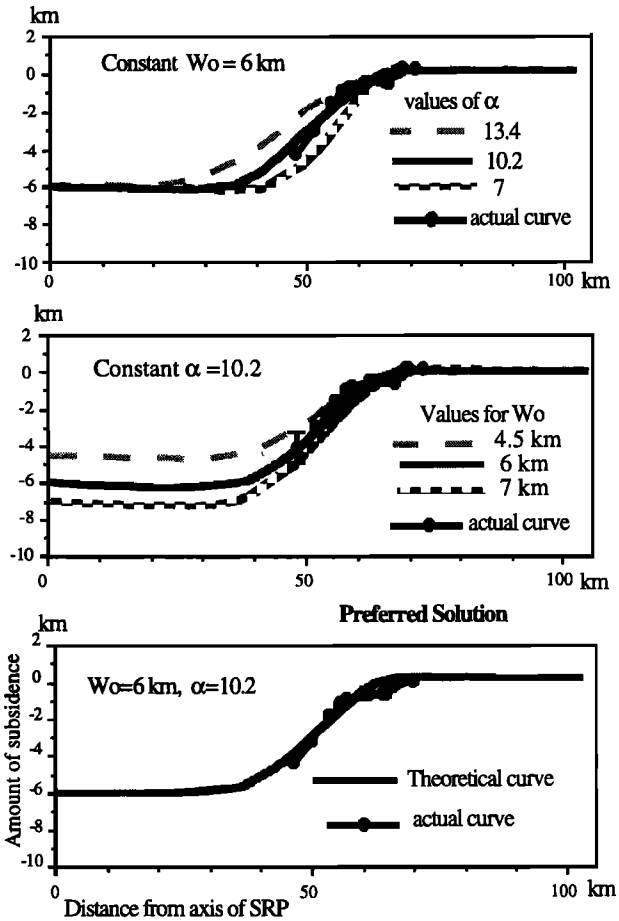

Figure 10. Actual and calculated flexure subsidence for the southern Beaverhead Range. Location of profile is shown in Figure 4. The half width of the midcrustal sill was varied between 30 and 60 km corresponding to a variation in α of 13.4- 7 km. The depth of the basin varied between 5 km and 7 km. Error bar shows a 1.5 km range in depths. The preferred solution is *Wo*= 6 km, *hL*= 17 km, α= 10.2 km, and *L*= 50 km.

with the observed Bouguer gravity on and near the ESRP. The ESRP gravity field has been characterized as an asymmetric positive anomaly roughly parallel with the ESRP [*LaFehr and Pakiser*, 1962; *Mabey*, 1978; *Eaton et al.*, 1978], with the strongest gravity gradient on the northwest side of the plain [*Sparlin et al.*, 1982]. The line of section used for two-dimensional modeling trends perpendicular to the length of the ESRP and is proximal to the Lost River Range, which is close to modeling lines chosen by *Sparlin et al.* [1982] but avoids a localized gravity high (Figure 13).

The gravity model (Figure 14) has blocks of varying density over a uniform mantle assuming isostatic compensation above 40 km. The model includes a 5 km deep basin and a 17 km thick midcrustal load with a density of 2.88 g cm^{-3}. This model is compatible with the positive gravity high along the axis of the ESRP, but to match the steep gravity gradient on the northwest flank lateral density contrasts are required in the upper through lower crust. To fit the sharp gravity gradient, *Sparlin et al.* [1982] thickened the lower crustal layer on the northwest side of the ESRP by lowering the Moho and decreasing the distance the midcrustal sill extends beyond the borders of the ESRP (Figure 6). An equally valid gravity model, and one that is preferred because it is compatible with a flat Moho and isostatic compensation above the mantle, involves a change in lower crustal density from 3.0 g cm^{-3} to 2.88 g cm^{-3} about 30 km north of the northern ESRP border (Figure 14). Independent seismic support for this transition is lacking because the velocity structure in the Basin and Range north of the ESRP below a few kilometers is poorly known [*Greensfelder*, 1981; *Peng*, 1996], but lower density (2.88 g cm^{-3}) lower crust is permissible based on lower crustal seismic velocities of 6.8 km s^{-1} obtained in southeastern Idaho and northern Utah [*Prodehl and Lipman*, 1989]. Geologically, the lower crustal density change would represent a contact between two different metamorphic rocks; as discussed below, this is preferred because of independent support for lower crustal flow from beneath the ESRP to the Basin and Range. In summary, the gravity model is not unique but indicates that the crustal layering determined by flexure modeling (Figure 11) is compatible with the regional gravity field.

7. Timing

The subsidence history of the ESRP is partly recorded by the age-depth relations of rhyolite ash flow tuffs in two drill holes located south of the Lemhi Range. INEL-1 is a 3159 m geothermal test well whose upper 745 m consist of basalt flows and intercalated sediments and whose lower 2414 m section consists exclusively of rhyolitic welded ash flow tuffs, air fall ash deposits, nonwelded ash flow tuffs, and volcaniclastic sediments [*Doherty et al.*, 1979]. The thickness and lithology of the rhyolitic rocks were interpreted to represent the fill of a collapsed caldera [*Doherty et al.*, 1979; *Morgan et al.*, 1984]. Lack of continuous core from the drill hole and extensive hydrothermal alteration complicates correlations with surficial rhyolite deposits, but core from the

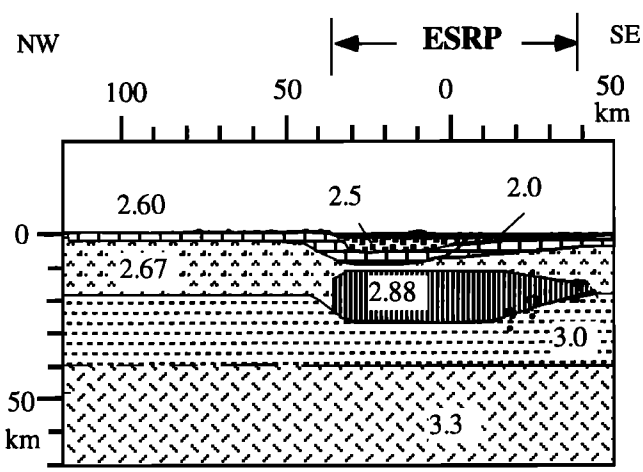

Figure 11. New lithospheric layering scheme for the ESRP showing Paleozoic crust downwarped beneath the volcanic basin. The midcrustal sill is thicker than that proposed by *Sparlin et al.* [1982] and is compensated in the lower crust. Densities are in g cm^{-3}.

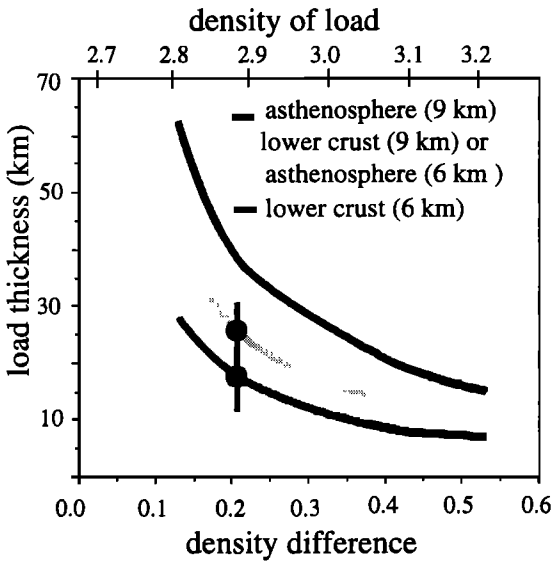

Figure 12. Relationship between load thickness and load density that would produce the preferred subsidence as constrained by the flexure equations. Circles indicate the preferred solutions for the Lost River Range (9 km of subsidence) and the Lemhi and Beaverhead Ranges (6 km of subsidence) with isostatic compensation in the lower crust.

drill hole located at a depth of 1500-2000 m was tenuously correlated with the 6.0 Ma tuff of Blue Creek based on petrographic similarities [*McBroome,* 1981; *Morgan et al.*, 1984]. Zircon fission track ages of the rhyolitic units in INEL 1 are 11.2 Ma at a depth of 3060 m, 8.8 Ma at a depth of ~2600 m, and 4.2 Ma at the basalt-rhyolite contact [*McBroome*, 1981; *Morgan et al.*, 1984]. In the second drill hole, WO-2, 1524 m of continuous rock core was logged. The bottom 380 m of the drill hole is composed of rhyolitic tuffs that were correlated with surficial exposures of the Heise Volcanic Group based on $^{40}Ar/^{39}Ar$ ages, paleomagnetic unit mean direction and feldspar geochemistry [*Hackett et al.*, 1994]. WO-2 contains the 4.3 Ma tuff of Kilgore, the 6.0 Ma tuff of Blue Creek, the 6.6 Ma tuff of Blacktail as well as previously unrecognized rhyolitic tuffs [*Hackett et al.*, 1994]. The tuff of Blacktail was logged at a depth of 1500 m (*Hackett et al.*, 1994). Because the tuff of Blacktail is exposed at Howe Point and because flexure data and modeling indicate a minimum of 5 km of subsidence beneath WO-2 (Figures 1 and 4), these data indicate that 3.5 km of subsidence predated the 6.6 Ma tuff of Blacktail.

Subsidence pre dating the tuff of Blacktail is supported by an angular unconformity. Folded Paleozoic rocks north of Howe Point show a consistent 20°± 3° (Figure 3) southward plunge. At Howe Point, the Paleozoic rocks are covered by Neogene rhyolites, but as described above, the compaction foliation of the tuff of Blacktail defines a curve whose southern limb is tilted 12° to the south, indicating 8° ± 3° of angularity across the unconformity. Significant subsidence prior to emplacement of the tuff of Blacktail conflicts with the major hypothesis of subsidence in the wake of the Yellowstone hotspot (YHS) [*Reilinger et al.*, 1977; *Brott et al.*, 1981; *Blackwell et al.*, 1992; *Anders and Sleep*, 1992; *Pierce and Morgan*, 1992] because the tuff of Blacktail is inferred to have erupted from a proximal vent located above the proposed YHS [*Morgan et al.*, 1984; *Pierce and Morgan*, 1992].

Figure 15 is a composite subsidence curve for the ESRP, based on subsidence analysis and drillhole information. Figure 15 shows three possible curves extrapolated to zero subsidence, initiating at 15, 13, and 10 Ma. Despite its rapid intial subsidence rate, the latter curve is preferred in this study because of changes in the style, amount, and expression of volcanism described below.

8. Discussion

8.1. Nature of the Load

In both flexure and gravity modeling, the midcrustal load was proposed to be a thick, rectangular, homogeneous load with a density of 2.88 g cm^{-3}. In reality, this load is more accurately envisioned as a composite of country rock and heterogeneous bodies (sills, dikes, and plutons) of varying densities that combine to produce the modeled load. Discrete reservoirs of magma within the load cooled and crystallized creating dense cumulates at the base of the magma chamber (M. McCurry, personal communication, 1997). The crystallization of magma reservoirs provided an increase in

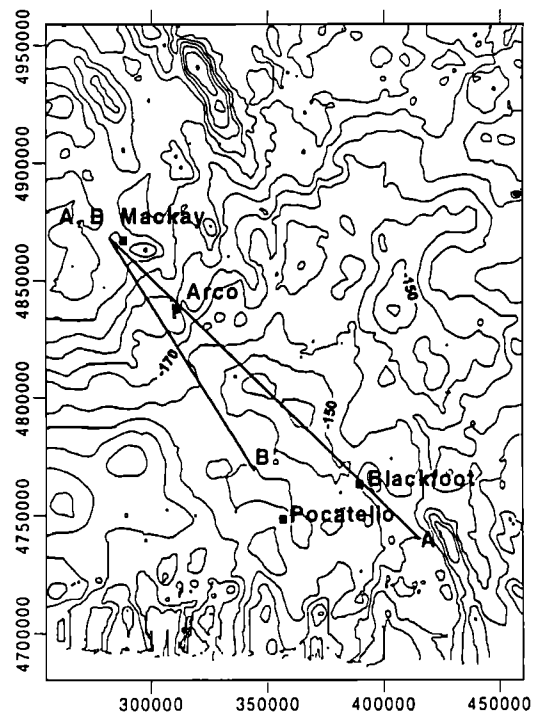

Figure 13. Bouguer gravity map of the ESRP with the lines of section from *Sparlin et al.* [1982] (A-A') and this study (B-B'). Map is referenced to the state plane coordinate system. Data for gravity map are after A.E. McCafferty, et. al. (Digital aeromagnetic, terrace- magnetization, Bouguer gravity, isostatic gravity, terrace-density, and topographic grids for data centered on the Idaho batholith, EROS data center release, magnetic tape, U.S. Geological Survey, 1990).
1990).

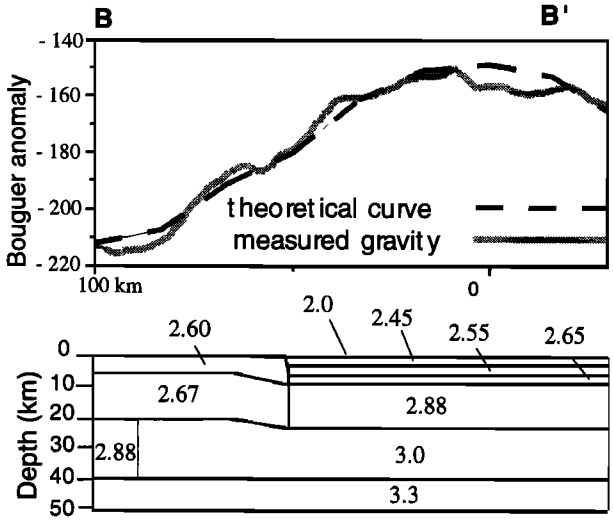

Figure 14. Gravity model along B-B' (Figure 13) varying density over a uniform mantle assuming isostatic compensation above 40 km. The model also includes a 5 km deep basin and a 17 km thick midcrustal load with a density of 2.88 g cm^{-3}. To model the steep northwest gravity gradient and maintain compensation above the mantle, a change in lower crustal density from 3.0 gm cm^{-3} to 2.88 g cm^{-3} is proposed 30 km north of the northern ESRP border.

density of the load and the heat necessary to melt the surrounding country rock and initiate volcanism [*Huppert and Sparks*, 1988]. Thus the proposed load is a combination of high-density (>2.88 g cm^{-3}) plutons and associated dikes and sills intruded into the lower-density country rock. The net effect is a load that can be modeled as a homogeneous rectangular body with the described dimensions and density.

8.2. Density driven lower crustal flow

In regions where the crust is hot, the weak lower crust flows in response to crustal loading [*Kaufman and Royden*, 1994] leaving isostasy completely compensated in the lower crust [*De Rito et al.*, 1986]. On the basis of the interpretation of seismic, heat flow, gravity, and flexure data (summarized in sections 5 and 6), we propose that the lower crust beneth the ESRP has flowed away from the ESRP and allowed density-driven subsidence of the ESRP upper crust. In this model, the ESRP and adjacent Basin and Range are initially in isostatic equilibrium, with the high elevation but lower density of the Basin and Range balanced by the higher density and low topography of the ESRP. Because isostatic disequilibrium leading to lower crustal flow can only be induced by processes that increase the mass of one column with respect to the other, we propose that the driving mechanism for lower crustal flow is the emplacement of dense magmas into the ESRP crust. In this model, the increase in mass drives lower crust outward to the Basin and Range and allows for load-induced subsidence of the ESRP as shown in Figure 16. A secondary mechanism that may accentuate flow is extension within the seismic parabola that fringes the ESRP (Figure 1). Extension should change mass by thinning the crust with respect to the ESRP and provide space for the influx of lower crust [*Kaufman and Royden*, 1994]. If this secondary mechanism is applicable, the outer edge of the seismic parabola may be a reasonable estimate of the stagnation point of flow.

This model differs from that proposed by *Anders and Sleep* [1992], who envisioned that lower crustal flow near the ESRP was driven by thermal contraction and expansion. In their model, the seismic parabola (Figure 1) is a topographic high due to thermal expansion of the lithosphere. The excess gravitational energy provided by topography is sufficient to drive lower crustal flow towards the ESRP, which owing to ongoing thermal contraction subsides and provides space for the influx of material. One problem with this model is that thermal contraction and expansion do not involve a change in mass. Because mass is conserved, a weight difference is not created, isostatic equilibrium is maintained, and there is no driving force for lower crustal flow toward the ESRP. A second problem is that although the excess topography of the seismic parabola should induce lower crust flow toward the ESRP, this model does not incorporate the differences in crustal density between the ESRP and the Basin and Range. For these reasons, we favor density-driven lower crustal flow away from the ESRP, rather than elevation-driven flow toward the ESRP.

One test of lower crustal flow is to establish the duration and range of inferred flow, use these data to calculate the required viscosity of lower crust, and determine if the viscosity is reasonable. Unreasonable viscosities would rule out lower crustal flow, whereas reasonable viscosities merely admit it is possible. *Kruse et al.* [1991] presented a lower crustal flow model which assumes Newtonian flow and includes as variables the lower crust viscosity, channel thickness, flow length, and duration of flow. For the ESRP region, the lower crustal "channel" is 15 km thick (the vertical distance between the Moho and the midcrustal sill) (Figure 11), the flow length ranges from 80 to 140 km (the distance from the edge of the ESRP to the outer parabola, as proposed above), and the flow duration is equal to the age of rhyolitic eruptions in the study area (Figure 17). Several transects from the border of the ESRP to the outer seismic parabola, combined with flow durations that range from 1 to 10 Ma consistently yield a lower crust viscosity of the order of 10^{17} Pa s, indicating that realistic variations in time and distance are not large enough to produce

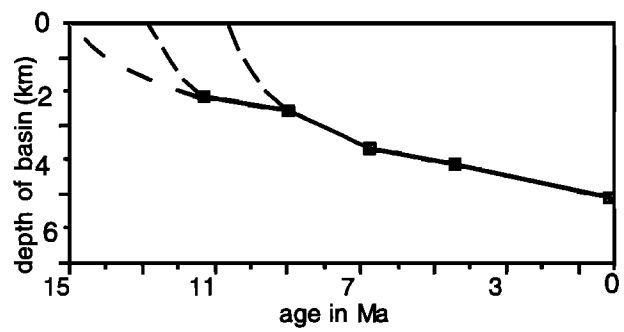

Figure 15. ESRP basin subsidence graph constrained by INEL-1 and WO-2 well log data, assuming 5 km of subsidence as documented by this study. Dashed lines represent three possible dates for initiation of subsidence. Data are from *McBroome* [1981], *Morgan et al.* [1984)], and *Hackett et al.* [1994].

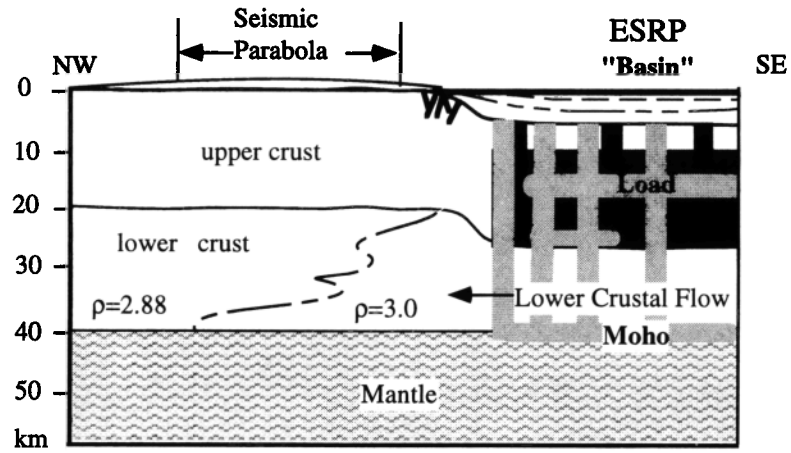

Figure 16. Summary Figure of ESRP and Basin and Range depicting features and timing of downwarping. These include (1) an extensive midcrustal load emplaced at ~10 Ma (solid area); (2) a post-Neogene load related to the volcanic rift zones (VRZ) (shaded area); (3) 5-8 km of downwarped Basin and Range crust; (4) a NE striking fault set due to flexure of the crust [*Zentner*, 1989b]; 5) an angular unconformity between the downwarped fold hinges and Heise volcanic rocks (dashed lines); (6) flat Moho; and (7) lower crustal flow from beneath the ESRP to the extending Basin and Range (seismic parabola).

a significant variation in viscosity. The ESRP lower crust viscosity is lower than viscosities of 10^{18} and 10^{21} Pa s determined for the Basin and Range Province [*Kruse et al.*, 1991] but is not unreasonable considering the high heat flow of the ESRP. We conclude that a low but reasonable viscosity of the lower crust would allow it to flow away from the ESRP into the adjacent Basin and Range.

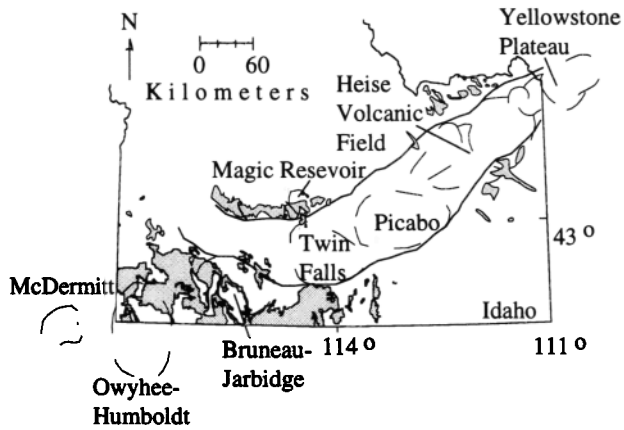

Figure 17. Rhyolite volcanic fields associated with the eastern Snake River Plain hotspot track from *Hughes et al.* [1996]. Modified from *Pierce and Morgan* [1992] with permission of the publisher, the Geological Society of America, Boulder, Colorado, USA, copyright © Geological Society of America. Shading is distribution of Tertiary rhyolite. Ages in Ma: Yellowstone Plateau, 1.3-0.6; Heise Volcanic Field, 4.3-6.6; Picabo, 10.2; Twin Falls, 8.6-10.02; Bruneau-Jarbidge, 12.5-11.3; Owyhee-Humboldt, 13.8-12.0; McDermitt, 16.1-15. Dates are from *Bonnichsen* [1982], *Bonnichsen et al.* [1988], *Christensen* [1984], *Ekren et al.* [1984], *Morgan et al.* [1984], *Rytuba and McKee* [1984], *Kellogg and Marvin* [1988], *Kellogg et al.* [1994], and *Perkins et al.* [1995].

8.3. Tectonic models of Subsidence

Time-transgressive development of the ESRP, as demonstrated by its southwestward topographic decline [*Reilinger et al.*, 1977; *Brott et al.*, 1981; *Anders and Sleep*, 1992] and its northeastward age progression of volcanism and faulting [*Armstrong et al.*, 1975; *Anders et al.*, 1989; *Rodgers et al.*, 1990; *Pierce and Morgan*, 1992], is not reflected in subsidence patterns. Over a distance of 150 km, the contour map of equal plunges (Figure 4) does not show a southwestward increase in subsidence amount or a consistent change in the width of the contours. Furthermore, initial subsidence was much earlier than passage over the YHS as inferred from rhyolite volcanism. Three hypotheses are presented to reconcile ESRP volcanism, subsidence, and deformation (Figure 16).

8.3.1. Relocation of vents for the Heise volcanic field. The Heise volcanic rocks logged in the WO-2 borehole do not show the lithological and structural features or the thickness associated with caldera fill deposits (although the complete character and thickness of the tuff of Blacktail is unknown), suggesting that the calderas associated with the Heise volcanic rocks are located farther northeast than initially proposed [*Anders et al.*, 1997]. In this case, the subsidence recognized in this study could have occurred southwest of major 6.6 Ma volcanism, in the wake of the YHS. The 6.6-4.3 Ma Heise volcanic rocks would have been deposited into an already subsiding basin. This revised model allows for subsidence due to cooling, injection, and densification in the wake of the hotspot and provides accommodation space for the preservation of the Heise volcanic rocks. However, this model fails to explain the preservation of 2-3 km of pre-6.6 Ma volcanic rocks identified in the subsurface at the INEL-1, rocks which are coeval with with the 10.2-8.6 Ma Twin Falls field located 100 km to the southwest. Preservation requires significant regional subsidence ahead of the YHS, for which there is no known mechanism.

8.3.2. Syneruptive subsidence of the Heise volcanic field. Oceanic hotspots are topographic highs due to both the building of a volcanic edifice and thermal expansion. However, most oceanic hotspots also show a crustal or structural subsidence associated with the weight of the volcanic load [*Crough*, 1978; *Sleep*, 1987; *Anders and Sleep*, 1992]. Therefore the volcanic islands are places of both topographic uplift and structural subsidence with initial subsidence during the emplacement of both intrusive magmas and extrusive volcanic rocks and continuing subsidence in the wake of the hotspot.

In contrast, structural subsidence around the Yellowstone plateau, an inferred continental hotspot, is not obvious. Mountain ranges composed of Paleozoic rocks continue unwarped to slightly upwarped (K. Pierce, personal communication, 1997) to the edge of the Yellowstone caldera. The magnitude of subsidence measured on the ESRP is not occurring at Yellowstone, suggesting syneruptive subsidence is not a dominant mechanism in this system.

8.3.3. Periodic late Cenozoic subsidence. Marked changes in the style and topographic expression of transgressive volcanism occurred at ~10 Ma [*Pierce and Morgan*, 1992](Figure 1). From about 16-10 Ma, eruption of high-temperature silicic volcanic rocks formed the Owyhee Plateau, whereas from about 10-4 Ma low-temperature silicic volcanic rocks accumulated in the ESRP volcanic basin. Older magmas rose west of the $^{87}Sr/^{86}Sr$ 0.706 isopleth through country rock dominated by accreted terranes, whereas younger magmas rose to the east through thicker crust dominated by Precambrian continental crust [*Pierce and Morgan*, 1992; *Leeman et al.*, 1992]. The frequency and amount of volcanic eruptions also declined at about 10 Ma [*Perkins et al.*, 1995; *Nash et al.*, 1993], although the extent of 10±1 Ma rhyolites increased significantly as shown by the 10.2 to 8.6 Ma Twin Falls and Picabo volcanic fields [*Pierce and Morgan*, 1992; *Perkins et al.*, 1995], the 10.3 Ma tuff of Arbon Valley possibly derived from the Tabor caldera, located near Blackfoot, Idaho (*Kellogg et al.*, 1994), the 11.2 and 8.8 Ma rhyolites identified in the INEL-1 drill hole [*Morgan et al.*, 1984], and the 9.9 Ma tuff of Kyle Canyon at Howe Point [*Morgan et al.*, 1984]. The widespread distribution of ~10 Ma volcanic rocks conflicts with the incremental, time transgressive volcanic system presented by most previous workers. To explain the widespread volcanism from Twin Falls to the Heise volcanic field, we propose that an extensive, linear pulse of mafic magmatism occurred at approximately 10 Ma beneath the ESRP. The magmatic pulse would have induced the extensive silicic volcanism throughout the region [*Leeman*, 1982a] and initiated widespread subsidence (Figure 16) by increasing the density of the middle crust.

Pierce and Morgan [1992] proposed that the change in volcanic style and topographic expression at ~10 Ma was due to the transition of the hotspot from a large bulbous head to a narrow linear tail or chimney [*Richards et al.*, 1989]. Alternatively, pre-10 Ma magmas may have ascended directly from the lower crust and experienced little to no residence time in the middle to upper crust [*Ekren et al.*, 1984] because of thinner, denser crust and/or high extension rates, whereas younger magmas may have coalesced in middle to upper crustal regions because of thicker, buoyant Precambrian crust and/or low extension rates [*Perkins et al.*, 1995; *Hughes et al.*, 1996].

After the initial pulse of subsidence at about 10 Ma, younger volcanic rocks represented by the Heise Volcanic Group (6.6-4.3 Ma) would have accumulated in an already subsiding ESRP basin (Figure 17). Their vents would be located northeast of INEL-1 [*Anders et al.*, 1997]. Presumably, this silicic volcanism was accompanied by additional injection of dense mafic magma, but existing age constraints cannot resolve a renewed pulse of subsidence at this time.

The alignment of basalt volcanic rift zones (VRZ) and recessions in the contour pattern (Figure 18) suggest that the ESRP "load" is not only Neogene but also includes a series of Quaternary dikes concentrated along the VRZ. Because these recessions record a northward shift in the locus of subsidence and not an increase in plunge amount, they are interpreted to be a result of extensions of the VRZ into the Basin and Range rather than an increase in the magnitude of the load. Two hypotheses are presented to explain the relationship between the Neogene and Quaternary loads. First, the Neogene midcrustal load may be the reservoir for Quaternary basalts and rhyolites. Experimental petrology suggests ESRP evolved basalts may be derived from olivine tholeiites in a middle to lower crustal reservoir [*Thompson*, 1975; *Leeman*, 1982b], and petrologic evidence suggests Quaternary rhyolites may be differentiated from these evolved basalts, implying large magma chambers at depth [*McCurry et al.*, 1997]. After Neogene rhyolitic volcanism ceased and the upper crust solidified and cooled, small percentages of mafic magma left in the midcrust could have risen through dikes and sills and been erupted from VRZ. In this case, the total load would be constant but redistributed. Second, ESRP tholeiitic basalt has a strong mantle signature and requires rapid ascent from the mantle [*Thompson*, 1975; *Kuntz* et al., 1992]; therefore these basalts should rise through the older load. In this case, the increase in density due to the plumbing system of the VRZ would be an additional load. The existence of both basalt types on the ESRP, the pattern of structural contours, and the few age constraints on loading suggest a combination of the two mechanisms.

8.4. Strength of the Interior Zone

An outstanding tectonic problem in the region is to explain the origin of the interior zone of the seismic parabola. The interior zone, which encompasses both the ESRP and sections of the adjacent Basin and Range, displays nearly uniform mechanical behavior characterized by subsidence and a lack of seismicity. To produce the observed mechanical behavior of the interior zone, workers have proposed it was strengthened or is a zone of low strain. *Anders et al.* [1989] and *Anders and Sleep* [1992] proposed that the seismically quiescent interior zone was strengthened by a midcrustal sill that extends to the inner border of the seismic parabola. The structural contour map of the flexed Basin and Range crust and the flexural modeling from this study indicate that the midcrustal sill extends only to the borders of the ESRP and cannot serve to strengthen the Basin and Range portion of the interior zone. This is also supported by a lack of volcanism [*Pierce and Morgan*, 1992] and a lack of increased heat flow [*Blackwell et al.*, 1992] north of the ESRP.

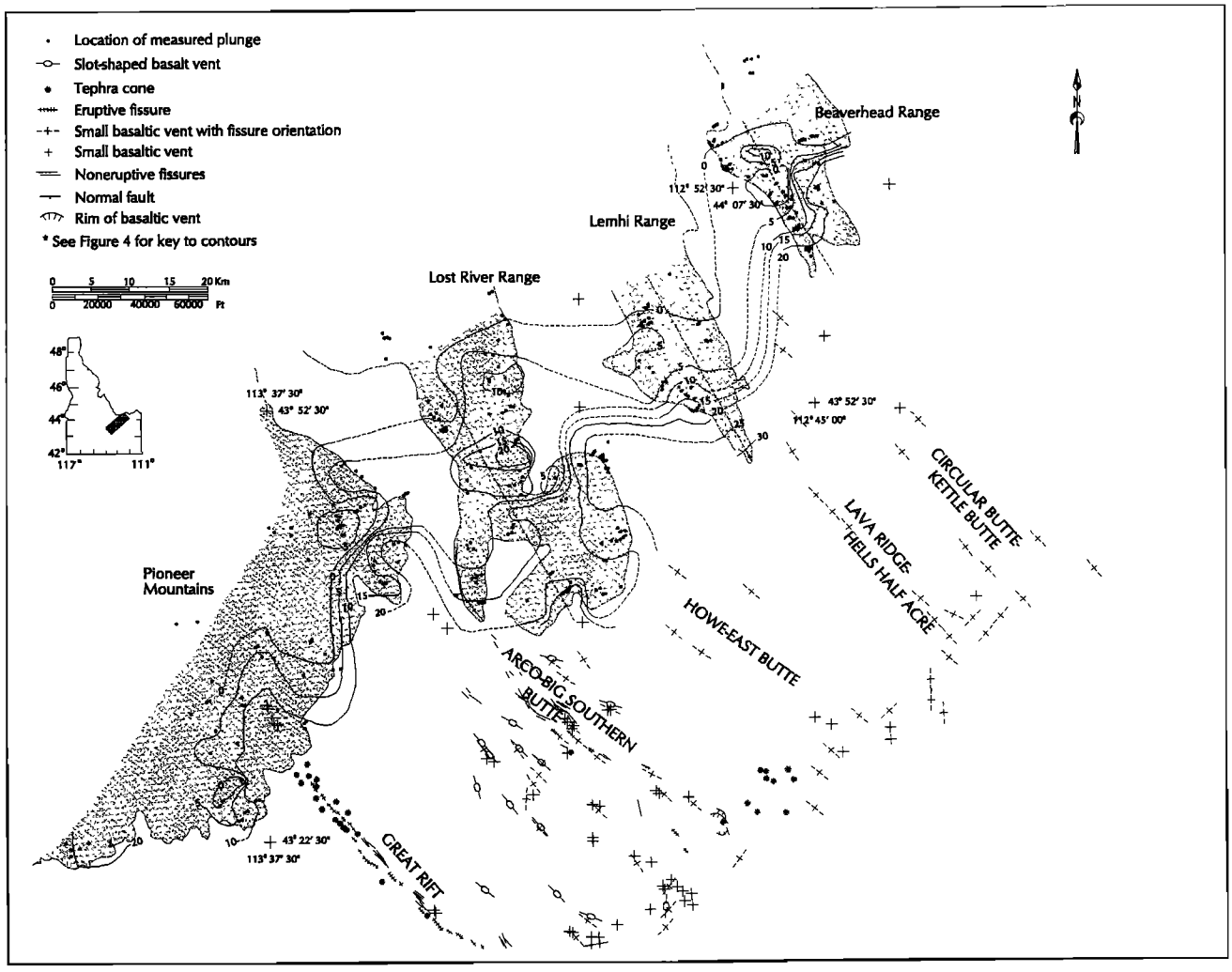

Figure 18. Spatial correlations between the downwarp contours and the volcanic rift zones of the eastern Snake River Plain. Where the rift zones are well defined (Arco and Great Rift areas), the correlations are very good. The lack of correlation to the northeast may reflect a poor understanding of rift zones in that area.

Suppression of earthquakes by magma overpressuring is another mechanism invoked to explain the seismically quiescent ESRP [*Parsons and Thompson*, 1991]. In extending terranes, mafic magma supplied at a pressure greater than the least principle stress decreases the differential stress and suppresses earthquakes. In this model, the lack of seismicity on the ESRP is tied directly to dike injection associated with rift zones. The correlation between the flexed crust and the VRZ presented in this study supports the importance of the VRZ in ESRP tectonics. As with a midcrustal sill that extends to the inner parabola, the lack of significant mafic magmatism off the ESRP suggests that magma overpressuring is not responsible for the quiescent Basin and Range adjacent to the ESRP. However, the interaction between the VRZ and the Basin and Range is seen in the pattern of downwarping (Figure 18), suggesting that there might be extensions of the VRZ in the Basin and Range that do not reach the surface.

9. Conclusions

1. The ESRP is a volcanic basin which subsided because of densification of the middle crust. Crustal flexure north of the ESRP is parallel to the axis of the ESRP, extends 10-20 km from the average edge, and indicates a minimum ESRP subsidence of 4.5-8.5 km. The measured flexure is compatible with a subsurface ESRP load with a thickness of 17-25 km, average density of 2.88 g cm^{-3}, and borders roughly coincident with the ESRP. Flexure modeling as well as seismic, gravity, and heat flow data strongly suggest that subsidence was compensated by density-driven lower crustal flow away from the ESRP.

2. Thermal contraction is a viable but insufficient subsidence mechanism for the ESRP because it cannot explain subsidence with respect to the Basin and Range. Further work is needed to identify the relative contributions of contraction and densification to overall subsidence.

3. Timing constraints require that more than half of the total subsidence of the ESRP occurred before 6.6 Ma. This suggests a significant load was emplaced at the initiation of rhyolitic volcanism at ~10 Ma. Correlation between Quaternary VRZ and flexure also suggests an additional load may be linked to the plumbing system for the recent basalt and evolved volcanics on the ESRP.

4. A spatially extensive pulse of volcanism at ~10 Ma suggests a change in rate, amount, and possible emplacement mechanism between the two eruptive centers. The rate of magmatism decreases dramatically between the extensive ~10 Ma volcanic field and Yellowstone. The amount of magmatism decreases sharply as well. The significance of these two changes suggest magmatism is not a perfect continuum along the ESRP. The ESRP-Yellowstone plateau system is broadly transgressive; however, additional work is needed to correlate the 8-10 Ma tuffs to volcanic centers and to reevaluate the rates of magma emplacement and subsequent rhyolitic volcanism.

5. There is not a direct relationship between the load (and the subsidence it produces) and the seismic parabola. Since the load does not extend past the ESRP borders, it is not directly responsible for strengthening the interior of the seismic parabola. Also significant is the lack of time-transgressive behavior shown by the measured subsidence and downwarping. Unless further investigation to the east and west reveals a time-transgressive pattern of subsidence, these data suggest that the seismic parabola is not a result of ESRP subsidence. However, the seismic parabola may be related to the ESRP by lower crustal flow from underneath the ESRP utilizing an already extending area.

6. The ESRP basin evolved in conjunction with the YHS, but current data indicate the ESRP basin originated above or ahead of the YHS, then continued to subside in its wake. Further resolution of the time-transgressive migration of the YHS is needed to specify the relative position of the ESRP basin through time.

Acknowledgments. This work was partially supported by a NSF/EPSCoR Graduate Assistantship and NASA-Idaho Space Grant Consortium Graduate Fellowship awarded to Nadine McQuarrie and a NASA-Idaho Space Grant Consortium minigrant awarded to David Rodgers. Discussions with Tom Ore, Mike McCurry, Glenn Thackray, and Clem Chase helped refine the ideas presented in this paper. We also acknowledge the very thoughtful and helpful reviews by Tom Parsons and Don Hyndman. Contributions to figures were provided by Ted Reid, Paul Wetmore, and Michelle Byrd.

References

Allen, P.A., and J R. Allen, *Basin Analysis, Principles and Applications*: Blackwell Sci. Cambridge, Mass., 451 pp., 1990.

Alt, D , J.M. Sears, and D.W. Hyndman, Terrestrial mana: The origins of large basalt plateaus, hotspot tracks and spreading ridges, *J. Geol., 96*, 647-662, 1988.

Alt, D , D.W., Hyndman, and J.M. Sears, Impact origin of late Miocene volcanism, Pacific Northwest, *Geol Soc. Am. Abstr. Programs, 22*, 2, 1990

Anders, M.H., J Saltzman, and W.R. Hackett, Borehole WO-2, the rosetta stone (core of the heise volcanics of east-central Idaho: Implications for the track of the Yellowstone hotspot, *Geol. Soc. Am. Abstr Programs, 29*, A-365, 1997.

Anders, M.H., and N.H. Sleep, Magmatism and extension: The thermal and mechanical effects of the Yellowstone hotspot, *J. Geophys. Res., 97*, 15,379-15,393, 1992.

Anders, M H., J.W Geissman, L.A. Piety, and J.T Sullivan, Parabolic distribution of circum-eastern Snake River Plain seismicity and latest Quaternary faulting. Migratory pattern and association with the Yellowstone hot spot, *J. Geophys. Res , 95*, 1589-1621, 1989.

Anders, M H., M. Spiegelman, D.W. Rodgers, and J.T Hagstrum, The growth of fault-bounded tilt blocks, *Tectonics, 12*, 1451-1459, 1993.

Angevine, C.L , P L. Heller, and C. Paola, Quantitative Sedimentary Basin Modeling, *AAPG Contin. Educ. Course Notes Ser., 32*, 132 pp., 1990.

Armstrong, F.C., and S.S. Oriel, Tectonic development of the Idaho-Wyoming thrust belt, *Am. Assoc Pet. Geol. Bull., 49*, 1847-1866, 1965.

Armstrong, R.L., W.P. Leeman, and H.E. Malde, K-Ar dating, Quaternary and Neogene volcanic rocks of the Snake River Plain, Idaho, *Am J. Sci., 275*, 225-251, 1975.

Beutner, E.C., Structure and tectonics of the southern Lemhi Range, Idaho, Ph D. thesis, 155 pp., P. State Univ., University Park, P., 1968.

Blackwell, D.D., S. Kelley, and J.L. Steele, Heat flow modeling of the Snake River Plain, Idaho, *U.S. Dep. of Energy Contr. Rep DE-AC07-761DO1570*, 109 pp., U.S. Dep. of Energy, Washington, D.C., 1992

Bonnichsen, B., The Bruneau-Jarbidge eruptive center, southwestern Idaho, in *Cenozoic Geology of Idaho*, edited by B. Bonnichsen and R.M. Breckenridge, *Bull.Idaho Bur. Mines Geol., 26*, 237-254, 1982.

Bonnichsen, B , W.P. Leeman, M.D. Jenks, and N Honjo, Geologic field trip to the central and western Snake River Plain, Idaho, emphasizing the silicic volcanic rocks, in *Guidebook to the Geology of Central and Southern Idaho*, edited by P.K. Link, and W.R. Hackett, *Bull. Idaho. Geol. Soc , 27*, 247-282, 1988.

Braile, L.W., R B. Smith, J. Ansorg, M.R. Baker, M A Sparlin, C. Prodehl, M.M. Schilly, J.H., Healy, St. Mueller, and K.H. Olsen, The Yellowstone-SRP seismic profiling experiment: Crustal structure of the eastern Snake River Plain, Idaho, *J Geophys. Res., 87*, 2597-2609, 1982.

Brott, C A., D.D Blackwell, and J.P. Ziagos, Thermal and tectonic implications of heat flow in the eastern Snake River Plain, Idaho, *J. Geophys Res., 86* , 11,709-11,734, 1981

Bruhn, R.L., D Wu, and J.J. Lee, Final report on structure of the southern Lemhi and Arco fault zone, Idaho, *Inf. Rep. Contrib. EGG-NPR-10680*, 25 pp., U.S. Dep. of Energy, Washington, D.C., 1992.

Busby, C J., and R V. Ingersoll, *Tectonics of Sedimentary Basins*: Blackwell Sci 579 pp., Cambridge, Mass., 1995.

Christiansen, R.L., Yellowstone magmatic evolution Its bearing on understanding large volume explosive volcanism, in *Explosive Volcanism· Inception, Evolution, Hazards*, pp. 84-95, Natl. Acad. Press, Washington, D. C., 1984.

Christiansen, R.L., and E.H. McKee, Late Cenozoic volcanic and tectonic evolution of the Great Basin and Columbia intermountain regions, in *Cenozoic Tectonics and Regional Geophysics of the Western Cordillera*, edited by R.B. Smith and G P. Eaton, *Mem.Geol. Soc Am. 152*, 283-311, 1978.

Crough, T.S., Thermal origin of mid-plate hot-spot swells, *Geophys. J. R. Astron. Soc., 55*, 451-469, 1978.

De Rito, R.F., F.A. Cozzarelli, and D.S. Hodge, A forward approach to the problem of nonlinear viscoelasticity and thickness of the mechanical lithosphere, *J. Geophys. Res., 91*, 8295-8313, 1986

Doherty, D.J., L.A. McBroome, and M.A. Kuntz, Preliminary geologic interpretation and lithological log of the exploratory test well (INEL-1), Idaho National Engineering Laboratory, eastern Snake River Plain, Idaho, *U S Geol. Surv. Open File Rep., 79-1248*, 10 pp., 1979.

Eaton, G.P., R.L. Christiansen, H.M Iyer, A.M. Pitt, D R. Mabey, H.R. Blank Jr., I. Zietz, and M.E Gettings, Magma beneath Yellowstone National Park, *Science, 188*, 787-796, 1975.

Eaton, G P., R.R. Wahl, H.L. Prostka, D.R. Mabey, and M.D. Kleinkopf, Regional gravity and tectonic patterns: their relation to late Cenozoic epeirogeny and lateral spreading in the western Cordillera, in *Cenozoic tectonics and regional geophysics of the western Cordillera*, edited by R.B Smith and G.P Eaton, *Mem. Geol. Soc. Am , 152*, 51-92, 1978.

Ekren, E B , D.H McIntyre, and E.H. Bennett, High-temperature, large volume, lavalike ash-flow tuffs without calderas in southwestern Idaho, *U.S. Geol. Surv. Prof. Pap., 1272*, 73 pp., 1984.

Fritz, W.J , and J.W. Sears, Tectonics of the Yellowstone hotspot wake in southwestern Montana, *Geology, 21*, 427-430, 1993.

Garmezy, L., Geology and tectonic evolution of the southern Beaverhead Range, east-central Idaho, M.S. thesis, 155 pp., P. State Univ., University Park, P., 1981

Greensfelder, R.W., Lithospheric structure of the eastern Snake River Plain, Idaho, Ph.D thesis, 188 pp. Stanford Univ , Stanford, Calif., 1981

Hackett, W.R, M.H. Anders, and R.C. Walter, Preliminary stratigraphic framework of rhyolites from corehole WO-2, Idaho National Engineering Laboratory: caldera-related, late-Tertiary silicic volcanism of the eastern Snake River Plain, paper presented at *VII International Symposium on the Observation of the Continental Crust Through Drilling*, Int. Cont. Drill. Program, Santa Fe, New Mexico, 1994.

Hamilton, W., Plate-tectonic evolution of the western U.S.A., *Episodes, 10* 271-276, 1987

Hamilton, W., Crustal geologic processes of the United States, in *Geophysical Framework of the Continental United States*, edited by L.C. Pakiser and W.D. Mooney, *Mem.Geol. Soc. Am, 172*, 743-781, 1989.

Hughes, S.S., J.L. Parker, A.M. Watkins, and M. McCurry, Geochemical evidence for a magmatic transition along the Yellowstone hotspot track, *Northwest Geol., 26*, 63-80, 1996.

Huppert, H.E., and R.S.J. Sparks, The generation of granitic magmas by intrusion of basalt into continental crust,*J. Petrol., 29*, 599-624, 1988.

Jackson, S.M., I.G. Wong, G.S. Carpenter, D.M., Anderson, and S.M. Martin, Contemporary seismicity in the eastern Snake River Plain, Idaho based on microearthquake monitoring, *Bull. Seismol. Soc. Am., 83*, 680-695, 1993.

Janecke, S.U., Kinematics and timing of three superposed extensional systems, east central Idaho: Evidence for an Eocene tectonic transition, *Tectonics*, 11, 1121-1138, 1992.

Johnson, R.W., *Intraplate Volcanism in Eastern Australia and New Zealand*, 408 pp., Cambridge Univ. Press, New York, 1989.

Kaufman, P.S, and L.H. Royden, Lower crustal flow in an extensional setting: Constraints from the Halloran Hills region eastern Mojave Desert, California, *J. Geophys. Res., 99*, 15,723-15,739, 1994.

Kellogg, K.S, and R F. Marvin, New potassium-argon ages, geochemistry, and tectonic setting of upper Cenozoic volcanic rocks near Blackfoot, Idaho, *U.S. Geol. Surv. Bull. 1806*, 19 pp., 1988.

Kellogg, K.S., S.S. Harlan, H.H. Mehnert, L.W. Snee, K.L. Pierce, W.R. Hackett, and D.W. Rodgers, Major 10.2-Ma rhyolitic volcanism in the eastern Snake River Plain, Idaho – Isotopic age and stratigraphic setting of the Arbon Valley Tuff Member of the Starlight Formation, *U.S. Geol. Surv. Bull., 2091*, 18 pp , 1994.

Kirkham, V.R.D., A geologic reconnaissance of Clark and Jefferson and parts of Butte, Custer, Fremont, Lemhi, and Madison Counties, Idaho, *Pam. Idaho Bur. Mines Geol., 19*, 47 pp., 1927.

Kirkham, V.R.D., Snake River downwarp, *J. Geol., 39*, 456-487, 1931.

Kruse, S., M. McNutt, J. Phipps-Morgan, L. Royden, and B. Wernicke, Lithospheric extension near Lake Mead, Nevada: a model for ductile flow in the lower crust: *J. Geophys. Res., 96*, 4435-4456, 1991

Kuntz, M.A., H.R, Covington, and L.J. Schoor, An overview of basaltic volcanism of the Eastern Snake River Plain, Idaho, in *Regional Geology of Eastern Idaho and Western Wyoming*, edited by P.K. Link, M.A. Kuntz, and L.B. Platt, *Mem. Geol. Soc. Am. 179*, 227-269, 1992.

Kuntz, M.A., et al., Geologic map of the Idaho National Engineering Laboratory and adjoining areas, eastern Idaho, scale 1:100,000, *U.S. Geol. Surv. Misc. Invest. Map, I-2330*, 1994a.

Kuntz, M.A., B. Skipp, and F.J. Moye, Preliminary geologic map of Craters of the Moon 30-x 60-minute quadrangle, Idaho, scale 1:100,000, *U.S. Geol. Surv. Open File Rep., 94-659*, 1994b.

LaFehr, T.R., and L.C. Pakiser,, Gravity, volcanism, and crustal deformation of the eastern Snake River Plain, *U.S. Geol. Surv.Prof. Pap.* 450-D, 76-78, 1962.

Leeman, W.P., Development of the Snake River Plain- Yellowstone Plateau province, Idaho and Wyoming: An overview and petrographic model, in *Cenozoic Geology of Idaho*, edited by B. Bonnichsen and R M. Breckenridge, *Bull. Idaho Bur. Mines Geol., 26*, 155-177, 1982a

Leeman, W.P., Evolved and hybrid lavas from the Snake River Plain, in *Cenozoic Geology of Idaho*, edited by B. Bonnichsen and R.M Breckenridge, *Bull Idaho Bur. Mines Geol, 26*, 193-202, 1982b.

Leeman, W P., J.S. Oldow, and W.K. Hart, Lithospheric-scale thrusting in the western U.S Cordillera as constrained by Sr and Nd isotopic transitions in Neogene volcanic rocks, *Geology, 20*, 63-66, 1992.

Lowry, A.R., and R.B. Smith , Strength and rheology of the western U.S. Cordillera, *J. Geophys. Res., 100*, 17,947-17,963, 1995.

Mabey, D.R., Regional gravity and magnetic anomalies in the eastern Snake River Plain, Idaho, *J. Res. U.S. Geol. Surv., 6*. 553-562, 1978.

Malde, H.E., Quaternary geology and structural history of the Snake River Plain, Idaho and Oregon, in *The Geology of North America*, vol. K-2,*Quaternary nonglacial geology of the Conterminous U.S.*, edited by R.B. Morrison, p. 251-281, Geol. Soc. of Am., Boulder, Colo., 1991.

McBroome, L.A., Stratigtraphy and origin of Neogene ash-flow tuffs on the northcentral margin of the eastern Snake River Plain, Idaho, M.S. thesis, 74 pp., Univ. Colo., Boulder, 1981.

McCurry, M., K Hayden, W.R. Hackett, and S. Mertzman, Petrology of Cedar Butte Volcano: implications for Quaternary high-silica rhyolite magmatism on the eastern Snake River Plain, in *Geological Society of America Fieldtrip Guide for the 1997 National Meeting*, edited by P.K. Link and B. Kowallis, *Brigham Young Univ. Geol. Stud. 42*, 9-20, 1997.

McIntyre, D H., E.D. Ekren, and R.F. Hardyman, Stratigraphic and structural framework of the Challis volcanics in the eastern half of the Challis 1° x 2° quadrangle, Idaho, in *Cenozoic Geology of Idaho*, edited by B. Bonnichsen and R M. Breckenridge, *Bull. Idaho Bur. Mines Geol, 26*, 155-177, 1982.

Morgan, L A., D.J. Doherty, and W.P. Leeman, Ignimbrites of the eastern Snake River Plain: Evidence for major caldera forming eruptions, *J. Geophys. Res., 89*, 8665-8678, 1984.

Morgan, W.J., Plate motions and deep mantle convection, *Mem. Geol. Soc. Am. 132*, 7-22, 1972.

Nash, W.P, M.E. Perkins, and F.H. Brown, Frequency and composition of explosive eruptions from the Yellowstone hotspot from 14-0 Ma, *Eos Trans. AGU, 25*, 593, 1993.

Nunn, J.A., and J.R. Aires, Gravity anomalies and flexure of the lithosphere at the Middle Amazon Basin, Brazil, *J. Geophys. Res., 93*, 415-428, 1988.

Parsons, T., and G.A. Thompson, The role of magma overpressuring in suppressing earthquakes and topography: worldwide examples, *Science, 253*, 1399-1402, 1991.

Peng, X., Crustal velocity structures inferred from waveform modeling of teleseismic waves: Studies of northern Nevada and the eastern Snake River Plain, Ph.D. thesis, 157 pp., Univ. of Oreg., Eugene, Oreg., 1996.

Perkins, M.E., W.P. Nash, F.H. Brown, and R.J. Fleck, Fallout tuffs of Trapper Creek, Idaho – A record of Miocene explosive volcanism in the Snake River Plain volcanic province, *U.S. Geol. Surv. Bull., 107*, 1484-1506, 1995.

Pierce, K L. and L.A. Morgan, The track of the Yellowstone hotspot: Volcanism, faulting and uplift, in *Regional Geology of Eastern Idaho and Western Wyoming*, edited by P.K. Link, M.A. Kuntz, and L.B. Platt, *Mem Geol. Soc. Am. 179*, 1-53, 1992.

Prodehl, C., and P W. Lipman, Crustal structure of the Rocky Mountain region, in*Geophysical Framework of the Continental United States*, edited by L C. Pakiser and W.D. Mooney, *Mem. Geol Soc. Am., 172*, 743-781, 1989.

Reilinger, R.E, G P Citron, and L D. Brown, Recent vertical crustal movements from precise leveling data in southwestern Montana, western Yellowstone National Park, and the Snake River Plain, J. *Geophys. Res., 82*, 5349-5359, 1977.

Richards, M.A., R.A. Duncan,, and V.E. Courtillot, Flood basalts and hot spot tracks: Plume heads and tails, *Science, 246*, 103-107, 1989.

Rodgers, D.W., and M H. Anders, Neogene evolution of Birch Creek Valley near Lone Pine, Idaho, in *Geologic Field Tours of Western Wyoming and Parts of Adjacent Idaho, Montana, and Utah*, edited by S. Roberts, *Public. Inf. Circ. Geol. Surv. Wyo., 29*., 27-40, 1990.

Rodgers, D.W., and S.U. Janecke, Tertiary paleogeographic maps of the western Idaho-Wyoming-Montana thrust belt, in *Regional Geology of Eastern Idaho and Western Wyoming*, edited by P.K. Link, M.A. Kuntz, and L.B. Platt, *Mem. Geol. Soc. Am. 179*, 83-94, 1992.

Rodgers, D.W., and N.C. Zentner, Fault geometries along the northern margin of the Eastern Snake River Plain, Idaho, *Geol. Soc. Am. Abstr. Programs, 20*, 465, 1988.

Rodgers, D.W., W.R. Hackett, and H.T Ore, Extension of the Yellowstone plateau, eastern Snake River Plain, and Owyhee plateau, *Geology, 18*, 1138-1141, 1990.

Rodgers, D W., H.T. Ore, R. Bobo, E P. Henderson, and A.D. Huerta, Drainage reversal in three Basin and Range grabens, southeastern Idaho Evidence for Miocene passage of the Yellowstone hot spot, *Geol. Soc. Am. Abstr. Programs*, 23, *88*, 1991.

Royse, F., Jr., M.A. Warner, and D.L. Reese, Thrust belt structural geometry and related stratigraphic problems, Wyoming-Idaho-northern Utah, in *Deep Drilling Frontiers of the Central Rocky Mountains*, edited by D.W. Bolyard, Rocky Mt Assoc of Geol., pp. 41-54, 1975.

Ruppel, E.T., Late Cenozoic drainage reversal, east-central Idaho, and its relation to possible undiscovered placer deposits, *Econ. Geol., 61*, 648-663, 1967.

Rytuba, J.J. and E.H. McKee, Peralkaline ash flow tuffs and calderas of the McDermitt volcanic field, southeastern Oregon and northcentral Nevada, *J. Geophys. Res., 89*, 8616-8628, 1984.

Schmidt, D.L., Quaternary geology of the Bellevue area in Blaine and Camas Counties, Idaho, *U S. Geol. Surv. Open File Rep. 625*, 133 pp., 1962.

Scott, W.E., Surficial geologic map of the eastern Snake River Plain and adjacent area, 111° to 115°W, Idaho and Wyoming, scale 1:125,000, *U.S. Geol. Surv Misc Investigations Map, I-1372*, 1982.

Scott, W.E., K.L. Pierce, and M H Hait Jr., Quaternary tectonic setting of the 1983 Borah Peak earthquake, central Idaho, in *Proceedings, Workshop XXVIII on the Borah Peak, Idaho, Earthquake*, edited by R.S. Stein and R.C. Bucknam, *U.S. Geol. Surv. Open File Rep., 85-290*, 1-16, 1985.

Skipp, B., Geologic map of Mackay 4 (Grouse) NE quadrangle, Butte and Custer Counties, Idaho, scale 1:24,000, *U.S Geol. Surv. Open File Rep.* 88-423, 1988.

Skipp, B., Geologic map of Mackay 4 (Grouse) NW quadrangle, Butte and Custer Counties, Idaho, scale 1:24,000, *U.S. Geol. Surv. Open File Rep.*, 89-142, 1989.

Skipp, B., and D.D. Bollmann, Geologic map of Blizzard Mountain North quadrangle, Butte and Custer Counties, Idaho, scale 1:24,000, *U.S. Geol. Surv. Open File Rep.*, 92-280, 1992.

Skipp, B., M.A. Kuntz, and L.A. Morgan, Geologic map of Mackay 4 (Grouse) SE quadrangle, Butte and Custer Counties, Idaho, scale 1:24,000, *U.S. Geol. Surv. Open File Rep.* 89-431, 1990.

Sleep, N.H., Lithospheric heating by mantle plumes, Geophys. J. R. Astron. Soc., *91*, 1-12, 1987.

Smith, R.B., W.C. Nagy, K.A., Julander, J.J. Viveiros, C.A., Barber, and D.G. Gants, Geophysical and Tectonic framework of the eastern Basin and Range - Colorado Plateau - Rocky Mountain transition, in *Geophysical Framework of the Continental United States:*, edited by Pakiser, L.C. and Mooney, W.D., *Mem. Geol. Soc. Am.*, *172*, 205-233, 1989.

Smith, R.B., W.D. Richins, and D.I. Doser, The 1983 Borah Peak, Idaho, earthquake: Regional seismicity, kinematics of faulting and tectonic mechanism, in *Proceedings, Workshop XXVIII on the Borah Peak, Idaho, Earthquake*, edited by R.S. Stein and R.C. Bucknam, *U.S. Geol. Surv. Open-File Rep. 85*-290, p. 236-263, 1985.

Sparlin, M.A., L.W. Braile, and R.B. Smith, Crustal structure of the eastern Snake River Plain determined from ray-tracing modeling of seismic refraction data, *J. Geophys. Res.*, *87*, 2619-2633, 1982.

Suppe, J., C. Powell, and R. Barry, Regional topography, seismicity, Quaternary volcanism, and the present day tectonics of the western United States, *Am. J Sci., 275-A*, 397-436, 1975.

Thompson, R.N., Primary basalts and magma genesis, II, Snake River Plain, Idaho, U.S.A., *Contrib. Mineral. Petrol.*, *52*, 213-232, 1975.

Turcotte, D.L., and G. Schubert, *Geodynamics: Applications of Continuum Physics to Geological Problems*, 450 pp., John Wiley, New York, 1982.

Turko, J.M., and P.L.K. Knuepfer, Late Quaternary fault segmentation from analysis of scarp morphology, *Geology*, *19*, 718-721, 1991.

Woodward, N.B., S.E., Boyer, and J. Suppe, *An Outline of Balanced Cross Sections*, Univ. Tenn. Dep. Geol. Sci Stud. Geol. vol. 11, 2nd ed., 170 pp., Univ. of Tenn., Knoxville, 1985.

Zentner, N.C., Neogene faults related to the subsidence of the Snake River Plain, *Geol. Soc. Am. Abstr. Programs, 21*, 162, 1989a.

Zentner, N.C., Neogene normal faults related to the structural origin of the eastern Snake River Plain, Idaho, M.S. thesis, 47 pp., Idaho State Univ., Pocatello, Idaho, 1989b.

N. McQuarrie, Department of Geoscienses, University of Arizona, Tucson, AZ 85721. (e-mail: nmcq@geo.arizona.edu)

D.W. Rodgers, Department of Geology, Idaho State University, Pocatello, ID 83209 (e-mail: rodgdavi@isu.edu)

(Recieved June 13, 1997;
revised December 3, 1997;
accepted December 29, 1997)